Cell Reports

Article

Differential translocation of bacteriophages across the intestinal barrier in health and Crohn's disease

Graphical abstract

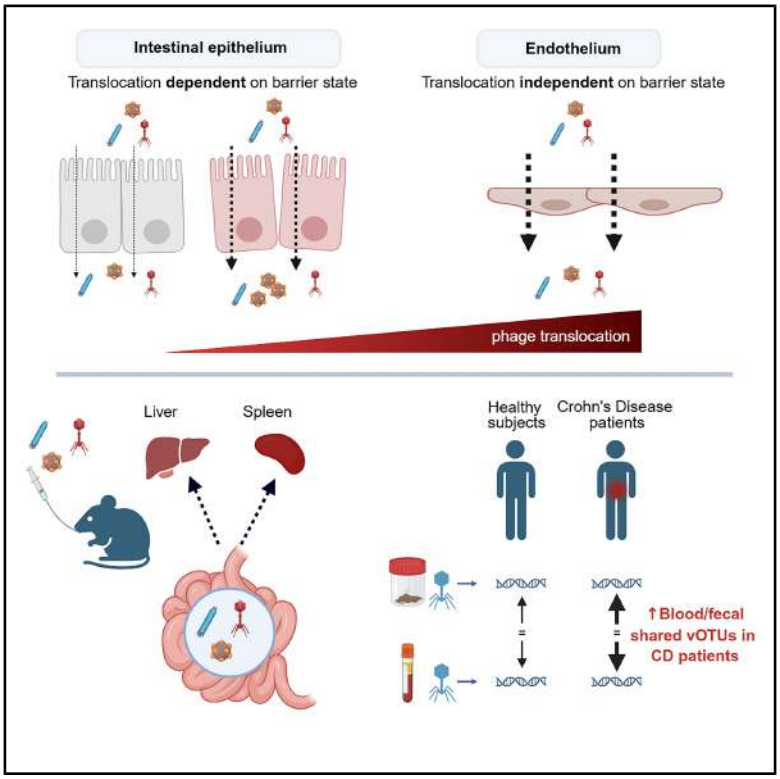

Authors

Clara Douadi, Quentin Lamy-Besnier, Ilias Theodorou, ..., Véronique Carrière, Sophie Thenet, Luisa De Sordi

Correspondence

luisa.de_sordi@sorbonne-universite.fr

In brief

Intestinal barrier integrity is crucial for gut homeostasis. Douadi et al. show that bacteriophages can cross this barrier without causing damage and that translocation rates depend on the barrier state. In Crohn's disease, impaired barrier function is associated with higher viral genomic sequences shared between feces and blood.

Highlights

- Bacteriophages cross the intestinal epithelium and endothelium at different rates
- Epithelial barrier alteration increases translocation of specific bacteriophages
- Intestinal bacteriophages translocate to the liver and spleen in mice
- Patients with Crohn's disease show increased sharing of gut and blood viral sequences

Douadi et al., 2026, Cell Reports *45*, 116726
January 27, 2026
https://doi.org/10.1016/j.celrep.2025.116726

CellPress

Cell Reports

CellPress
OPEN ACCESS

Article

Differential translocation of bacteriophages across the intestinal barrier in health and Crohn's disease

Clara Douadi,[1,2] Quentin Lamy-Besnier,[1,3] Ilias Theodorou,[1,3] Olivier Schiettekatte,[1] Yanis Sbardella,[1,2] Loïc Brot,[1,2] Paolo Emidio Costantini,[4,5] Roberto Saporetti,[5,6] Alberto Danielli,[4,5] Matteo Calvaresi,[5,6] Marianne De Paepe,[3] Harry Sokol,[1,2,3,7] Diego Garcia-Weber,[1,2,8] Véronique Carrière,[1,2,9] Sophie Thenet,[1,2,8,9] and Luisa De Sordi[1,2,9,10,*]

[1]Sorbonne Université, INSERM, Centre de Recherche St Antoine, 75012 Paris, France
[2]Gut, Liver & Microbiome Research (GLIMMER) FHU, Paris, France
[3]Université Paris-Saclay, INRAE, AgroParisTech, Micalis Institute, Jouy-en-Josas, France
[4]Dipartimento di Farmacia e Biotecnologie (FaBiT) – Alma Mater Studiorum - Università di Bologna, Bologna, Italy
[5]IRCCS Azienda Ospedaliero-Universitaria di Bologna, Bologna, Italy
[6]Dipartimento di Chimica "Giacomo Ciamician" – Alma Mater Studiorum - Università di Bologna, Bologna, Italy
[7]AP-HP, Saint Antoine Hospital, Gastroenterology Department, 75012 Paris, France
[8]EPHE, PSL University, Paris, France
[9]These authors contributed equally
[10]Lead contact
*Correspondence: luisa.de_sordi@sorbonne-universite.fr
https://doi.org/10.1016/j.celrep.2025.116726

SUMMARY

Impaired intestinal barrier function is a major feature of Crohn's disease, leading to exacerbated inflammation in response to the microbiota. In this context, the translocation of intestinal bacteriophages (phages) and their effects on the host haven't been fully investigated. We use phage fluorescence imaging coupled with *ex vivo*, *in vitro*, and *in vivo* models that mimic physiological and inflammatory conditions and find that phages can translocate across the intestinal barrier without disrupting its integrity. While changes in the epithelial barrier integrity selectively impact phage translocation rates, alterations in the permeability of the vascular endothelium do not affect phage crossing. Virome analysis confirms that viral sequences shared between the blood and fecal samples of patients with Crohn's disease are more abundant than in healthy subjects, suggesting that a barrier defect facilitates intestinal phage translocation.

INTRODUCTION

The intestinal mucosa plays a crucial role in preventing the invasion of luminal microbiota, acting as an essential barrier function for the body, in addition to nutrient absorption and endocrine functions.[1] The maintenance of intestinal barrier integrity results from the combined efforts of specialized epithelial and endothelial cells, as well as immune cells and accessory cells such as enteric glial cells and pericytes. The epithelial barrier consists of a monolayer of tightly sealed differentiated cells lining the gut lumen, which are coated with a layer of mucus and maintained together by an apical junctional complex comprising tight junctions, adherens junctions, and desmosomes.[2] The endothelial barrier, forming a deeper layer of protection located in the mucosa and submucosa, is composed of endothelial cells that line the interior of intestinal capillaries and blood vessels.[3] These cells are interconnected by tight and adherens junctions, creating an additional obstacle to be crossed to reach the bloodstream and distant organs.[4] Both the epithelial and endothelial barriers are semi-permeable and essential for regulating the exchange of molecules and fluids from the intestinal lumen into the circulation. An imbalance in their structure can allow unrestrained crossing of microbial components from the intestinal lumen, triggering an excessive immune reaction. An impaired intestinal barrier has been reported in a wide array of human diseases, both extraintestinal,[5–8] such as multiple sclerosis and non-alcoholic fatty liver disease, and intestinal, including inflammatory bowel disease (IBD).

Crohn's disease, one of the two main types of IBD, is characterized by chronic relapsing inflammation of the gastrointestinal tract (GIT), leading to bowel damage and a reduced quality of life for patients.[9,10] Crohn's disease is considered to be due to an abnormal immune response against the gut microbiota in patients with genetic predispositions and influenced by environmental factors, resulting in chronic inflammation.[11–13] In addition, Crohn's disease is associated with a local loss of the mucus layer,[14] increased intestinal permeability,[14–17] and endothelial dysfunction.[18,19] These harmful defects facilitate the passage of bacteria or their products from the GIT into systemic circulation.[20–23] Furthermore, the increased recruitment of leukocytes in the lamina propria may lead to the local

Table 1. Characteristics of the phages used in the study

Phage	Family	Size	Bacterial host
T4	Straboviridae	length: 200 nm width: 90 nm	*E. coli* K-12 MG1655
M13	Inoviridae	length: ±900 nm width: 7 nm	*E. coli* K-12 MG1655 F+
ΦX174	Microviridae	diameter: 25 nm	*E. coli* C+

accumulation of pro-inflammatory mediators, such as inflammatory cytokines, further exacerbating intestinal barrier failure.[24,25]

Bacteriophages (phages) are the most abundant viruses of the gut microbiota, representing between 10^9 and 10^{10} virus-like particles (VLPs) per gram of feces,[26] and are strongly suspected to have a role in shaping gut bacterial communities.[27] Although several early metagenomic studies reported that the gut phageome differs between patients with Crohn's disease and healthy subjects (HSs),[28–30] it has more recently been shown that the intestinal phageome lacks reliable markers for Crohn's disease due to its immense diversity and interpersonal variability.[31,32] Phages have been shown to interact with mammalian cells, including intestinal epithelial cells, macrophages, and endothelial cells.[33–38] Nonetheless, their translocation across the gut barrier and their effects on its function and inflammation remain largely unknown.

Here, we investigated the interaction of phages with the intestinal barrier under both physiological and inflammatory conditions. Using a combination of *ex vivo*, *in vitro*, and *in vivo* models, we addressed whether phages of varying sizes and structures can translocate from the gut to other tissues and whether they, by themselves, induce deleterious effects. We demonstrate that a fraction of all tested phages translocates across the intestinal epithelium and endothelium without disrupting the integrity of these barriers or triggering an inflammatory response. In mice, we confirmed that functional phages can rapidly translocate across the intestinal barrier. Furthermore, analysis of the viral genomic sequences shared between the blood and the stool of the same subject suggests higher phage translocation in patients with Crohn's disease.

RESULTS

Phages translocate across intestinal epithelial cells without disrupting barrier integrity

As the epithelial barrier is the first interface for the intestinal microbiota, we studied the interaction of phages with this barrier using an *in vitro* Caco-2/TC7 cell model that closely reproduces most of the morphological and functional characteristics of normal human absorptive enterocytes.[39,40] Initially, we ensured that neither Caco-2/TC7 basal culture medium (Figure S1A) nor 1% Triton X-100, used for cell lysis (Figure S1B), directly affected phage viability. T4, M13, and ΦX174 phages, each belonging to distinct families with different structures and sizes (Table 1), along with the fluorescent tracer FD4, were introduced into the apical compartment at the beginning of the experiment (Figure 1A).

After 2 h of incubation, only M13 phages were detected in the basal medium (data not shown). However, after 4 h, all three phages were recovered in the basal medium, with the rate of M13 translocation being significantly higher than that of T4 (Figure S2A). After 24 h, phage translocation increased approximately 10-fold relative to that after 4 h. Depending on the phage, 0.0035%–0.02% successfully translocated across the monolayer, and between 0.44% and 2.2% were found to be associated with intestinal epithelial cells (Figure 1B). M13 phages showed higher cell association and translocation rates compared to the other two phages (Figure 1B), suggesting that the translocation process may differ between phage types. Furthermore, we found no correlation between the initial phage dose and translocation efficiency, indicating that translocation is not a dose-dependent process but is likely limited by the epithelial barrier (Figure S2B).

We explored the localization of M13 phages to better understand how they translocate through the epithelial barrier by covalently conjugating them with CF488 fluorophores and following them by confocal microscopy. After 24 h, M13 phage particles were colocalized with actin of the microvilli, both as aggregates and isolated phages, leading to an average of 4% of cells positive for CF488 labeling (Figures 1C and 1D). Large aggregates of M13 phage particles on intestinal epithelial cells were 16-fold less frequent than isolated phages (Figure 1D). Examination along the *yz* axis confirmed that M13 phage particles were located at the level of microvilli, which were revealed by actin staining, with a weak proportion internalized within intestinal epithelial cells (Figure 1E). They were also visualized below the epithelial monolayer, in accordance with our titration of phages in the basal medium, demonstrating that functional phages are able to cross the epithelial barrier (Figure 1E). We then examined whether M13 phages could also translocate through the intestinal epithelium using paracellular pathways. We labeled tight and adherens junction proteins and observed colocalizations between M13 phage particles and the junction proteins tricellulin, ZO-1, and E-cadherin, suggesting that phages can also be associated with intercellular junctions, although such subcellular localization was not predominant (Figure 1F).

We assessed whether phages are damaged during translocation across the epithelial barrier by quantifying T4 phage particles, both by plaque assays and qPCR. There were no differences between plaque-forming unit (PFU) counts and quantification by qPCR, indicating that most translocated phages remain functional (Figure S2C).

No differences in epithelial barrier integrity were observed between Caco-2/TC7 cells incubated with or without phages (control [CTL]), as measured by FD4 flux, trans-epithelial electrical resistance (TEER), lactate dehydrogenase (LDH) release, and interleukin (IL)-8 pro-inflammatory chemokine secretion (Figures S2D–S2G), indicating that phages do not induce hyperpermeability, cytotoxicity, or inflammation.

These findings provide evidence that under physiological conditions, all three studied phages can translocate across intestinal epithelial cells without disrupting the barrier function.

Phages internalize by endocytosis and translocate across endothelial cells without disrupting barrier integrity

Next, we investigated the fate of phages after their translocation across the epithelial barrier, hypothesizing that they might reach

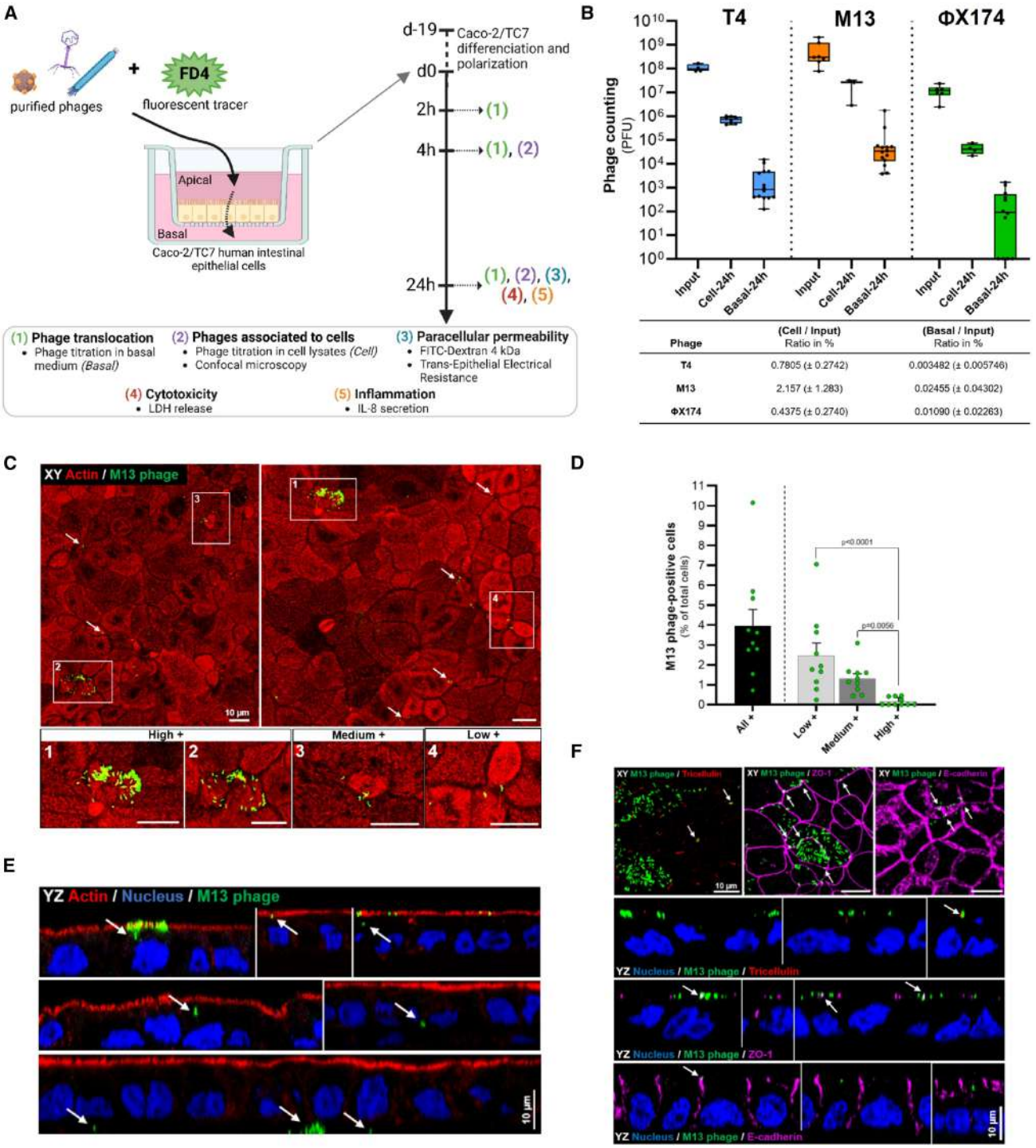

Phage	(Cell / Input) Ratio in %	(Basal / Input) Ratio in %
T4	0.7805 (± 0.2742)	0.003482 (± 0.005746)
M13	2.157 (± 1.283)	0.02455 (± 0.04302)
ΦX174	0.4375 (± 0.2740)	0.01090 (± 0.02263)

Figure 1. Internalization and translocation of phages across human intestinal epithelial cells

(A) Overview of the experimental setup: T4, M13, or ΦX174 phages and the fluorescent tracer FD4 were added to the apical compartment of Caco-2/TC7 cells cultured in transwell filters. Samples were collected at 2, 4, and 24 h to investigate the phage association with cells, phage translocation, paracellular permeability, cytotoxicity, and inflammation.

(B) Titration of T4, M13, and ΦX174 associated with Caco-2/TC7 cells (cell) and translocated through the monolayer (basal) after 24 h of incubation. The input refers to the phages initially added to the apical compartment. A minimum of four independent experiments ($n \geq 4$) was performed. The table displays the percentage of phages associated with cells and translocated across Caco-2/TC7, calculated relative to the input.

(legend continued on next page)

the bloodstream via intestinal capillaries. To test this, we investigated phage interactions with the endothelial barrier that lines these vessels.

Human umbilical vein endothelial cells (HUVECs) were cultured on a permeable membrane to establish a confluent monolayer. T4, M13, or ΦX174 phages and the fluorescent tracer FD4 were introduced into the apical compartment (Figure 2A). We first ensured that the HUVEC basal culture medium did not directly affect phage viability (Figure S1C). All phages showed a high level of translocation across HUVECs within 1 h. Notably, only ΦX174 phages showed a significant further increase after 24 h, and no significant difference was observed between the three phages (Figure 2B). The translocation rates of T4, M13, and ΦX174 across the endothelial barrier were 346-, 285-, and 806-fold higher, respectively, than those across the epithelial barrier (Figures 1B and 2B). These results indicate that phages can cross the endothelial barrier, regardless of the phage type, and thus may be able to reach the bloodstream.

We then investigated the mechanism by which phages translocate across the endothelial barrier, hypothesizing that they are internalized through endocytosis. We introduced CF488-labeled M13 phage particles (Figure 2A) and observed significant accumulation within HUVECs from 30 min to 24 h, with perinuclear localization (Figures 2C and 2D), showing that HUVECs are highly permeable to phages. We compared the intracellular trafficking of fluorescent M13 phage particles with that of Cy3-labeled transferrin, used as an endocytosis cargo control,[41] at both 37°C and 4°C (the latter temperature being known to inhibit endocytosis). M13 phage particles and Cy3-labeled transferrin were simultaneously introduced onto a HUVEC monolayer (Figure 2A). We observed a strong fluorescent transferrin signal within the HUVECs from 30 min up to 4 h of incubation at 37°C, confirming, as expected, its internalization by endocytosis (Figures S3A and S3B; Figures 2E and 2F). By contrast, after 30 min of incubation at 37°C, the fluorescent M13 phage signal was weak (Figures S3A–S3C), indicating that transferrin appears to be internalized more rapidly than M13 within HUVECs. After 1–4 h of incubation, robust colocalization was observed between transferrin and M13 phage particles, suggesting their convergence within the endocytic pathway (Figures S3A and 2E). Importantly, both intracellular transferrin and M13 phage signals were much weaker at 4°C than 37°C (Figures S3A–S3C, 2E, and 2F), indicating that M13 is internalized through an active endocytic process. No significant colocalization was detected over time between M13 phage particles and LysoTracker, which labels acidic compartments (Figures 2G and S3D), suggesting that most phages evade lysosomal degradation.

Furthermore, none of the tested phages modified the permeability of the endothelial barrier by themselves as assessed by xCELLigence, FD4 passage, or TEER (Figures S3E–S3H).

Overall, these results show that phages can easily translocate across the endothelial barrier through endocytosis and without inducing deleterious effects, thus demonstrating their potential to efficiently reach the bloodstream.

A compromised intestinal barrier facilitates phage ΦX174 translocation but has no impact on M13 or T4 translocation

Crohn's disease is associated with a defect in the intestinal barrier, notably characterized by increased intestinal permeability.[2,17,25] We explored whether such hyperpermeability could lead to higher phage translocation by mimicking alterations of intestinal epithelial and endothelial barriers *in vitro*.

First, Caco-2/TC7 cells were treated with either EGTA to globally disorganize cell-cell junctions or pro-inflammatory cytokines to trigger an inflammatory condition, before introducing phages (Figure 3A). As expected, interferon gamma (IFNγ) + tumor necrosis factor alpha (TNF-α) and EGTA altered epithelial barrier function (Figures S4A and S4B) by significantly increasing paracellular permeability, with EGTA having a more pronounced effect than the cytokines (Figures S4A and S4B). IFNγ + TNF-α treatment also led to a significant increase in cytotoxicity relative to the control and EGTA conditions, and both treatments increased IL-8 secretion (Figures S4C and S4D). EGTA treatment significantly increased the translocation of ΦX174 compared to the control and IFNγ + TNF-α conditions, whereas the translocation of M13 and T4 was not modified (Figure 3B). Furthermore, ΦX174 translocation significantly correlated with paracellular permeability, whereas no such correlation was observed for T4 or M13 (Figure 3D; Table 2). Similar to the physiological context, under compromised barrier conditions, there were no differences between PFU counts and quantification by qPCR, suggesting that most translocated phages remain functional and that barrier defects do not affect phage infectivity (Figure S2C).

In addition, in Caco-2/TC7 cells under compromised barrier conditions, ΦX174 phages did not induce hyperpermeability (Figure 3C; Table S1) or cytotoxicity (Figure S4I) or exacerbate inflammation (Figure S4L). Similar results were observed for T4 (Figures S4E, S4G, and S4J; Table S1) and M13 (Figures S4F, S4H, and S4K; Table S1), indicating that when barrier integrity is compromised, phages do not trigger further deleterious effects upon translocation.

We then assessed the impact of an endothelial barrier defect on phage translocation. HUVECs were incubated with IFNγ

(C) Images of CF488-labeled M13 phages interacting with Caco-2/TC7 cells following 24 h. Examples of high+, medium+, and low+ fields are shown in the insets, corresponding to different fluorescence levels of Caco-2/TC7 positive for CF488-labeled M13 phages.
(D) Quantification of the percentage of Caco-2/TC7 cells positive for CF488-labeled M13 phages, as shown in (C). Cells were categorized based on the fluorescence intensity of phages from an analysis of 10 randomly selected images (see the STAR Methods section).
(E) *yz* views of CF488-labeled M13 with Caco-2/TC7 cells after 24 h.
(F) Images (*xy* and *yz* views) of CF488-labeled M13 phages combined with immunofluorescence stainings of tricellulin (tight junctions), Zonula Occludens-1 (ZO-1; tight junctions), and E-cadherin (adherens junctions) after 24 h.
In all fluorescence images, M13 phages are covalently conjugated with CF488 fluorophore (green), actin is labeled with Alexa A546-phalloidin (red), and nuclei are labeled with DAPI (blue). The white arrows indicate phages colocalizing with actin (C), tricellulin (F), ZO-1 (F), and E-cadherin (F) or internalized within cells (E). Scale bar, 10 μm. Graphs (B) and (D) were analyzed for significance using the Kruskal-Wallis test. Data are represented as the mean ± SEM.

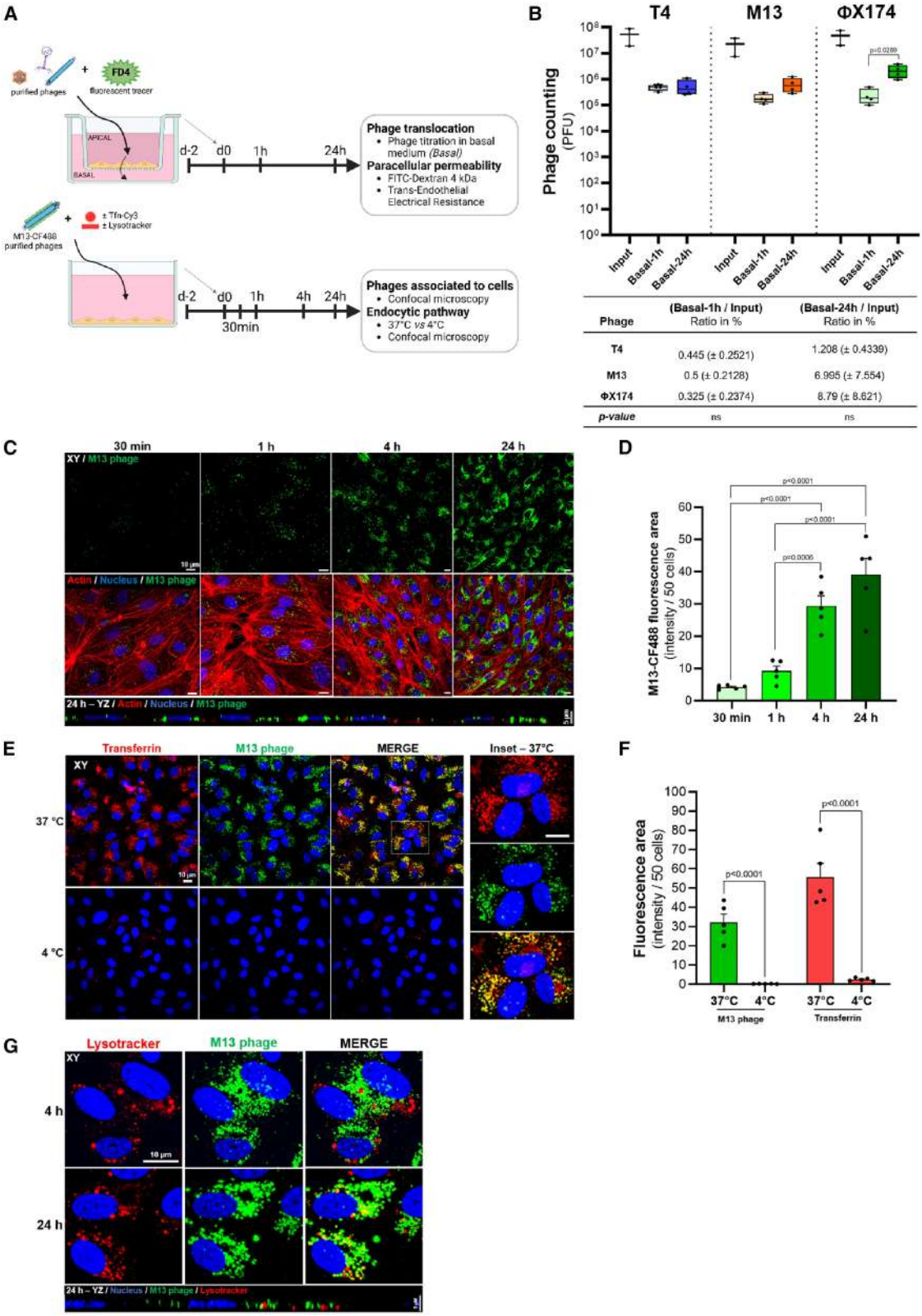

Phage	(Basal-1h / Input) Ratio in %	(Basal-24h / Input) Ratio in %
T4	0.445 (± 0.2521)	1.208 (± 0.4339)
M13	0.5 (± 0.2128)	6.995 (± 7.554)
ΦX174	0.325 (± 0.2374)	8.79 (± 8.621)
p-value	ns	ns

(legend on next page)

and TNF-α to mimic an inflammatory condition. Such treatment resulted in a significant increase in FD4 flux and a decrease in TEER (Figures S5A and S5B) without inducing LDH release (Figure S5C), showing that, as expected, pro-inflammatory cytokines increase the paracellular permeability of the endothelial barrier without inducing cytotoxicity. The endothelial barrier defect did not affect the translocation rate of T4, M13, or ΦX174 (Figures S5D–S5F), suggesting that phages do not mainly translocate across the endothelial barrier through the paracellular pathway.

Overall, these findings show that inflammatory conditions have no impact on phage translocation through the endothelial barrier but do facilitate the translocation of ΦX174 phages across the epithelium.

Phages can cross the intestinal barrier in healthy and inflamed mice

Following *in vitro* evidence that phages can translocate across both intact and compromised intestinal barriers, we first investigated their ability to cross entire mouse intestinal tissues using the Ussing chamber system. The translocation capacity of T4, M13, and ΦX174 was measured in the basal (serosal) compartment 90 min after their addition to the apical (luminal) compartment, along with the fluorescent tracer FD4 (Figure 4A). FD4 flux averaged 0.03% in the ileum and 0.018% in the colon, indicating that both intestinal tissues remained viable and undamaged throughout the experiment (Figure S6A). As expected,[42–44] ileal permeability was approximately twice that of the colon (Figure S6A). Remarkably, 10^2–10^4 PFUs of all tested phages demonstrated the capacity to cross the mouse ileum sections, retaining the ability to infect bacteria and form plaques (Figures 4B–4D), with translocation rates ranging from 0.000093% to 0.00041% (Table S2). Translocation of functional T4 and M13 was also observed across the colon (Figures 4B and 4C) but not for ΦX174 (Figure 4D).

We next evaluated whether phage translocation also occurs *in vivo* in both physiological and pathological contexts. C57BL/6J wild-type (WT) mice were provided either water or 2% DSS in drinking water for 7 days to induce intestinal inflammation. On day 9, mice were orally gavaged with 4.45×10^9 PFUs of T4, M13, and ΦX174 phages (Figures 4E and S6E) and sacrificed 1 or 5 h later. The small intestine, colon, liver, spleen, and feces were collected for phage quantification by plaque assay. DSS-treated mice showed significant clinical signs of inflammation (Figures S6B–S6D). At both 1 and 5 h post-gavage, phages were detected in the small intestine, colon, and feces (Figures S6F and S6G), confirming their transit through the GIT. As expected, no phages were observed in WT mice that did not receive the phage cocktail (data not shown). Detection of M13 was not possible in extraintestinal organs due to technical limitations, but ΦX174 was found in the liver and spleen of both control and DSS-treated mice as early as 1 h post-gavage (Figure 4F). T4 was also detected in the liver of some animals (Figure S6H).

Together, these findings demonstrate that a small fraction of functional phages can rapidly translocate from the lumen across the intestinal barrier in mice, regardless of inflammatory status, while the extent and kinetics of this translocation need further investigation.

Patients with Crohn's disease exhibit a signal of higher translocation of phages from the gut to the blood, including those of the Microviridae family

We then investigated whether our findings extended to pathological conditions characterized by gut barrier deficiency. We used viral metagenomics (viromics) to study phage translocation from the intestinal lumen to the bloodstream in a cohort of patients with Crohn's disease for whom the fecal and blood viromes were characterized.[32] We considered viral (phage) sequences retrieved from both fecal and blood samples as a signal of gut-blood translocation and specifically asked whether these sequences were quantitatively and qualitatively different in health and disease.

Blood and fecal samples were collected from 15 patients with Crohn's disease and 14 HSs (Table S3). Viral metagenomes were prepared, sequenced, and analyzed using a dedicated pipeline developed for this purpose (Figure 5A). Due to the low viral load in the blood, we applied stringent filters to ensure reliable detection of viral operational taxonomic units (vOTUs): each nucleotide of the vOTU must be sequenced at least once (depth $\geq$ 1), and a minimum 50% of its sequence must be covered (coverage $\geq$5 0%). Only the vOTUs passing both criteria were considered present in a sample, resulting in a total of 16,970 high-confidence vOTUs. A complete analysis of these samples is reported in a separate study from our laboratory.[32]

We first examined the overlap between vOTUs present in each sample type to identify candidates for phage translocation.

Figure 2. Internalization of phages through endocytosis and translocation across human endothelial cells

(A) Overview of the experimental setup: T4, M13, or ΦX174 phages and the fluorescent tracer FD4 were applied to HUVECs cultured either on transwell filters or a glass coverslip. Samples were collected at 30 min and/or 1, 4, or 24 h to evaluate phage translocation, paracellular permeability, phage association with cells, and phage internalization via the endocytic pathway.

(B) Titration of T4, M13, and ΦX174 in the basal compartment (basal) after 1 and 24 h. The input refers to the phages initially added to the apical compartment. The table displays the percentage of translocated phages across HUVECs, calculated relative to the input.

(C) Images of CF488-labeled M13 phages with HUVECs after 30 min and 1, 4, and 24 h of incubation. Actin was labeled with Alexa A546-phalloidin (red), and nuclei were labeled with DAPI (blue). The *yz* view corresponds to 24 h of incubation.

(D) Quantification of the M13-CF488 fluorescence shown in (C). Data were obtained from the analysis of 5 randomly selected images.

(E) Images of CF488-labeled M13 phages and Cy3-labeled transferrin in HUVECs after 4 h at 37°C or 4°C.

(F) Quantification of the red fluorescence area (transferrin) and green fluorescence area (M13 phages) in HUVECs following 4 h at 37°C or 4°C, as shown in (E). Data were obtained from the analysis of 5 randomly selected images.

(G) Images of CF488-labeled M13 phages and LysoTracker deep red in HUVECs after 4 and 24 h. The *yz* view corresponds to 24 h of incubation.

Scale bars of all *xy* views, 10 μm. Scale bar of all *yz* views, 5 μm. Graph (B) was analyzed for statistical significance using the Kruskal-Wallis test, graph (D) using ordinary one-way ANOVA, and graph (F) using Student's *t* test. Data are represented as the mean ± SEM.

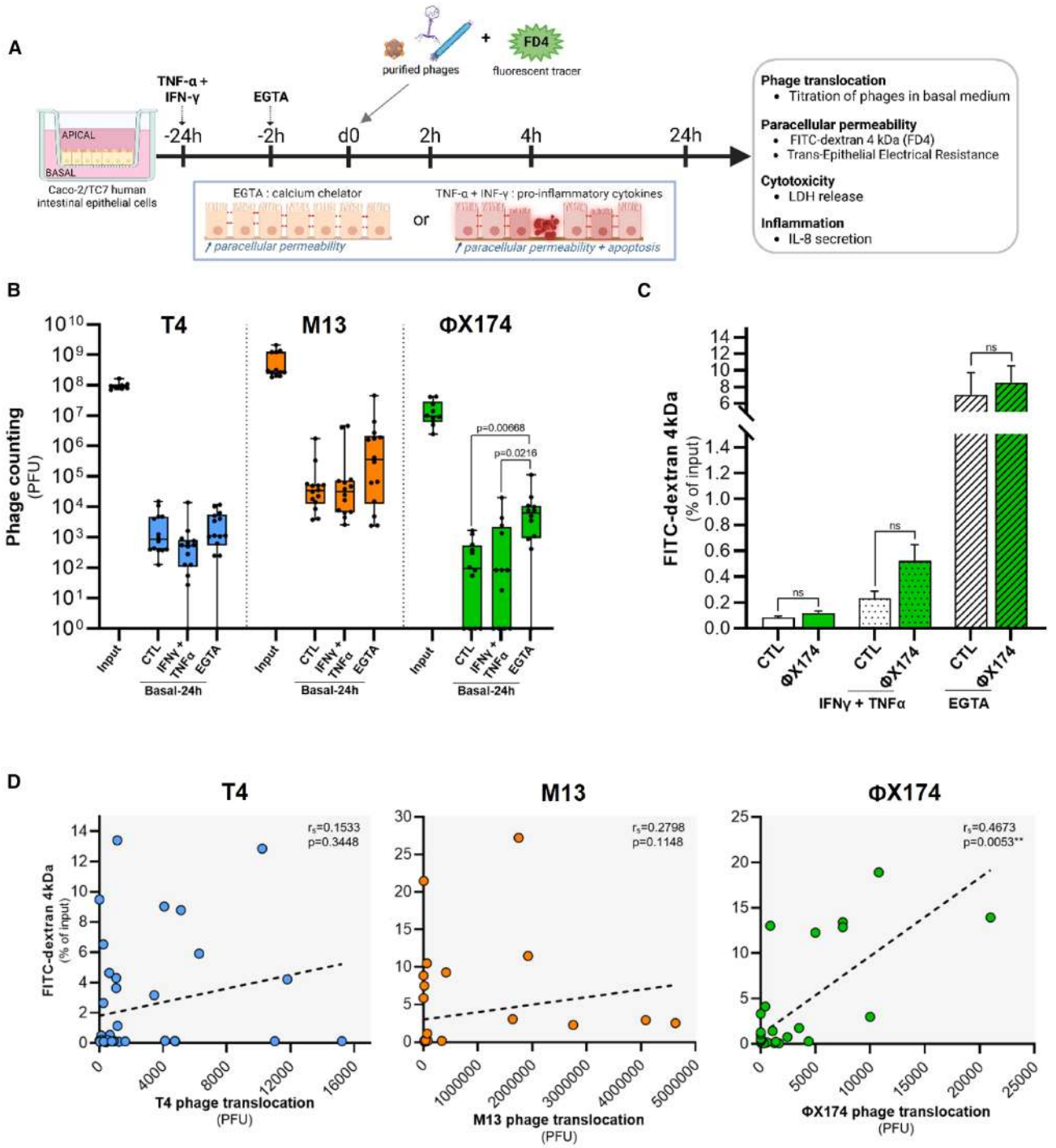

Figure 3. A compromised intestinal barrier facilitates ΦX174 translocation across intestinal epithelial cells

(A) Overview of the experimental setup: pro-inflammatory cytokines or EGTA was applied to the basal or apical compartment, respectively, of Caco-2/TC7 cells cultured on transwell filters to increase paracellular permeability. T4, M13, or ΦX174 phages and the fluorescent tracer FD4 were then added to the apical compartment. Samples were collected at 2, 4, and 24 h.

(B) Titration of T4, M13, and ΦX174 in the basal compartment (basal) after 24 h of incubation. The input refers to the phages initially added to the apical compartment. Conditions include healthy barrier conditions (CTL) relative to compromised barrier conditions (IFNγ + TNF-α or EGTA).

(legend continued on next page)

Across all 29 subjects, 14,843 vOTUs were found exclusively in stool, whereas 1,746 were unique to blood (Figure S7A). A total of 48 identical vOTUs (0.3% of total vOTUs) were detected in both fecal and blood samples, regardless of whether they originated from the same subject (Figure S7A).

Then, to specifically investigate the role of the gut barrier, we focused on the subset of vOTUs simultaneously detected in both blood and fecal samples retrieved from the same subject (Figure 5A). This targeted analysis identified 16 such blood/fecal shared vOTUs (Table S4). Patients with Crohn's disease had significantly more of these blood/fecal shared vOTUs than HSs, indicative of a potential increase in phage translocation from the intestinal lumen to the bloodstream (Figure 5B). Since most vOTUs correspond to phages, we identified their predicted bacterial hosts to trace their origin. Of the 16 vOTUs shared between blood and fecal samples, six infected hosts belonged to the phylum Bacillota (previously known as Firmicutes), and three infected hosts belonged to the phylum Bacteroidota (previously Bacteroidetes), which are the two most abundant phyla in the human gut microbiota,[45] suggesting a gut origin for these phages (Figure 5C). Together, these findings support the hypothesis that phage translocation from the gut to the bloodstream is increased in patients, but this should be validated by isolation of functional phages in future studies.

Given our previous observation that ΦX174 translocation is higher when the intestinal barrier is impaired in the Caco-2/TC7 model, we postulated that Microviridae phages may be more likely to cross the gut and reach the bloodstream. From the total 16,970 vOTU dataset (blood and stool), 211 Microviridae vOTUs were identified, accounting for 1.3% of vOTUs (Figure 5D). All 29 subjects harbored Microviridae in their fecal samples, as expected, totaling 210 vOTUs (Figure 5D). Notably, there was no difference in Microviridae diversity or relative abundance between patients with Crohn's disease and HSs in fecal samples (Figures S7B and S7C). Of the 5 Microviridae vOTUs identified in blood samples from the 29 subjects, 4 were also detected in fecal samples, highlighting their presence in both compartments (Figure 5D). These 4 vOTUs were distributed across two patients and one HS. This overlap shows that most Microviridae found in blood are also present in stool, pointing to a likely intestinal origin. Supporting this, the four blood Microviridae vOTUs for which we could predict the bacterial host infect phyla that are prevalent in the human gut microbiota (Figure 5E).

In addition, among the 16 blood/fecal shared vOTUs retrieved from the same subject, three belong to Microviridae, representing approximately 19% of the potentially translocated vOTUs (Table S4). These three Microviridae vOTUs originated from patients with Crohn's disease and showed a strong gut association (>90% average nucleotide identity homology against gut virus databases; see the STAR Methods and Table S4). Despite the low number of Microviridae vOTUs, the 15-fold enrichment compared to the 1.3% prevalence of Microviridae in our full dataset of 16,970 vOTUs suggests that, within this cohort, phages from the Microviridae family may have a higher propensity to cross the intestinal barrier and reach the bloodstream.

Overall, our virome analysis supports intestinal phage translocation and proposes that this process is more frequent in patients affected by impaired gut barrier function. Additionally, Microviridae phages might be more prone to this translocation, warranting further investigation in a larger cohort.

DISCUSSION

Although a few studies have recently highlighted the interaction of phages with various cell types,[33–38] such interactions are still poorly understood in both physiological and disease contexts.

Despite the tightly regulated nature of the intestinal epithelial barrier, we observed that phages can translocate across the intestinal epithelium at different rates. Similarly, recent studies reported minimal translocation of *E. coli* phages through intestinal epithelial cells,[34] suggesting a size-dependent process,[33,35] but we cannot exclude that factors such as capsid charge or receptor-binding proteins may also play a role. Further studies using a broader range of phages and controlled comparisons are necessary to clarify the relative contributions of size, morphology, and other intrinsic properties. Our study simultaneously compares phages with such distinct morphologies, i.e., filamentous Inoviridae, caudated Straboviridae, and the smaller Microviridae. In the physiological context, we observed a higher level of translocation for M13, suggesting a better translocation capacity for Inoviridae than for Straboviridae and Microviridae. Fluorescently tagged phages were observed at the microvilli, internalized within and crossing the intestinal epithelium. Although rare, we noted aggregates of M13 phages on intestinal epithelial cells, a phenomenon not observed on endothelial cells. The mechanisms underlying such aggregation are unknown, but possibilities include a specific cellular signal that triggers phage aggregation or trapping within the microvilli. In addition, an active process induced by phages is possible, as M13 phages have been shown to increase gene expression of integrins when interacting with specific human cells.[46] Phage translocation across human cells is suggested to be vectorized from the apical to the basal side,[35,47] and, based on microscopy images, we suggest that microvilli could serve as gateways for phages to internalize via transcytosis. For example, phages might interact with cell surface proteins that share structural similarities with bacterial phage receptors.[38] Another possibility is the potential for phages such as M13, which are approximately 6 nm in diameter,[48] to use paracellular pathways. We found the phages to be rarely associated with tight and adherens junctions. Although our current data do not allow a definitive answer, we hypothesize that M13 phages may primarily use the transcytosis pathway, as demonstrated in other cell lines.[49]

(C) FD4 passage from the apical to the basal compartment during 24 h in the presence of ΦX174 phages compared to control without phages (CTL) conditions under healthy and compromised barrier conditions (IFNγ + TNF-α or EGTA).

(D) Correlation analysis between the translocation rates of T4, M13, or ΦX174 phages in all conditions (CTL, EGTA, and IFNγ + TNF-α) and FD4 flux.

For all experiments, a minimum of four independent experiments ($n \geq 4$) was performed. Graphs (B) and (C) were analyzed for statistical significance using the Kruskal-Wallis test and graph (D) using Spearman's test. Data are represented as the mean ± SEM.

Table 2. Correlations between phage translocation and TEER, LDH release, or IL-8 secretion in Caco-2/TC7 cells

	TEER		LDH release		IL-8 secretion	
Phage	Corr. coeff r_s	*p* value	Corr. coeff r_s	*p* value	Corr. coeff r_s	*p* value
T4	−0.1219	0.4418	−0.04722	0.7665	0.03693	0.8164
M13	−0.2919	0.0841	0.05567	0.7262	0.07097	0.7094
ΦX174	−0.7469	<0.0001	0.1254	0.4729	0.2584	0.1339

Correlation analyses were performed between the translocation rates of T4, M13, or ΦX174 in all conditions (CTL, EGTA, and IFNγ + TNF-α) and TEER, LDH release, or IL-8 secretion. Spearman's test was used to assess the correlation between the two variables tested.

Our study demonstrates that phages interact with the endothelial barrier in a markedly different way than with the epithelial barrier. Endothelial cells were over 500 times more permeable to phages, and this translocation occurred independently of phage type. Highly polarized epithelial cells, which form a selective barrier, contrast sharply with gut vascular endothelial cells, which have fewer and more loosely organized tight junctions, leading to greater permeability.[3] Supporting our findings, small macromolecules, such as those of approximately 4 kDa, can easily diffuse through the endothelial barrier into the bloodstream,[50] whereas intestinal epithelial cells restrict their passage.[51,52] We also found that M13 phages are internalized by endothelial cells through endocytosis, a process confirmed by other studies in different cell types.[33,35,38,49] Phage internalization in the endothelial barrier appears to be active, but the exact endocytic pathway involved is still unclear.[53] According to Tian et al., the size of M13 filamentous phages may be compatible with macropinocytosis,[49] but T4 and ΦX174 phages could use different endocytic pathways.

Pharmacokinetic studies have detected phages in the bloodstream of mice, highlighting their ability to cross biological barriers,[54–56] and a parallel study from our team estimated that ~20% of circulating phages may originate from the gut.[32] Our study provides mechanistic insight into this process,

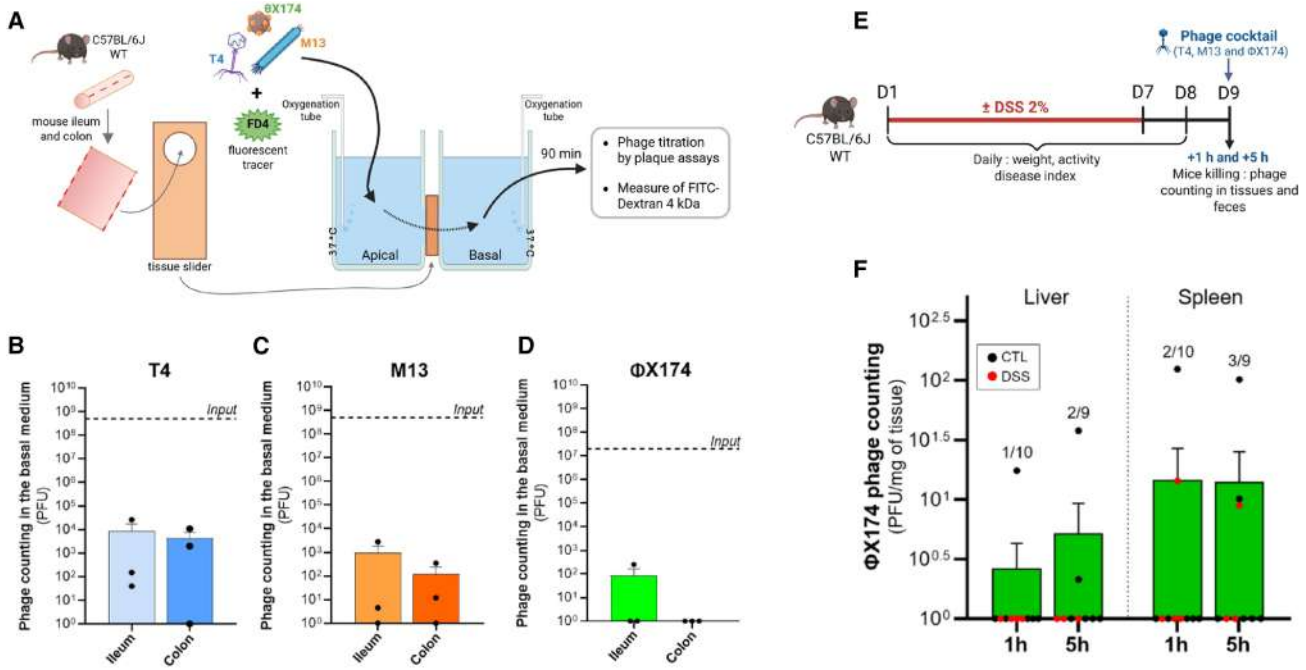

Figure 4. Translocation of phages across the intestinal barrier in mice

(A) Overview of Ussing chamber experimental setup: T4, M13, or ΦX174 phages and the fluorescent tracer FD4 were added to the apical side. Samples from the basal compartment were collected to assess paracellular permeability and phage translocation.

(B–D) Translocation of T4 (B), M13 (C), or ΦX174 (D) across mouse ileum and colon tissues 90 min after apical addition. For each phage condition, three ileum or colon tissue samples (obtained from two or three individual mice) were analyzed. The phage quantity initially added to the apical chamber is indicated with the dotted line (input).

(E) Overview of *in vivo* experimental setup: C57BL/6J WT mice were treated or not with 2% DSS for 7 days. On day 9, mice received a phage cocktail by oral gavage and were sacrificed either 1 or 5 h post-gavage. Phage quantification was performed in tissues (small intestine, colon, liver, and spleen) and feces.

(F) Titration of ΦX174 in liver and spleen by plaque assays, in control and DSS-treated mice, 1 or 5 h after oral administration. $n = 6$ mice per control group and $n = 3$ or 4 mice per DSS-treated group. The numbers indicate mice positive for phage detection in the liver or spleen out of the total tested. All graphs were analyzed for statistical significance using the Mann-Whitney test. Data are represented as the mean ± SEM.

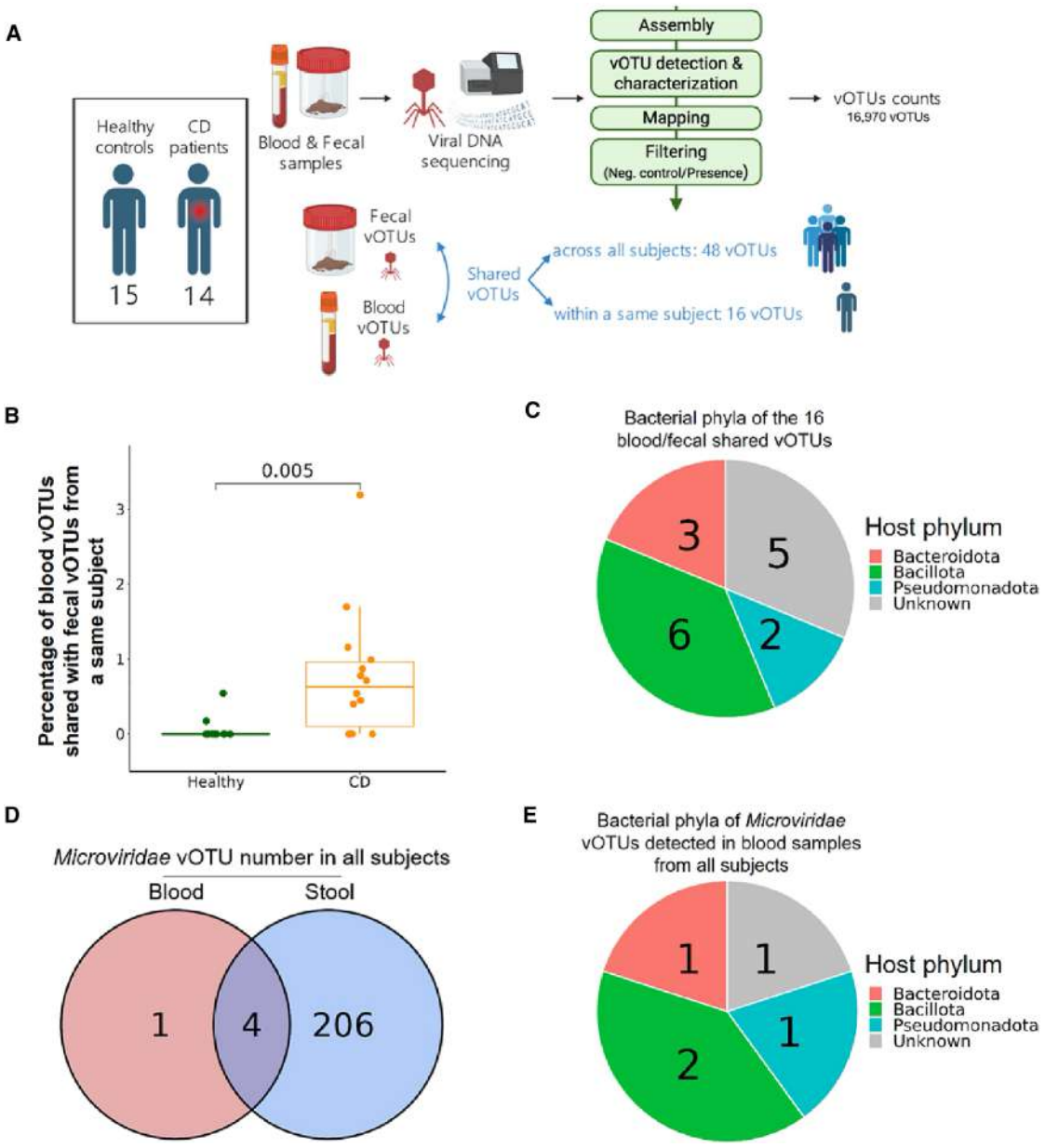

Figure 5. Analysis of shared fecal and blood viromes in healthy subjects and patients with Crohn's disease

(A) Overview of the cohort sample collection and experimental setup: viral DNA from healthy subjects and patients with Crohn's disease (CD) was extracted, sequenced, and analyzed through a dedicated pipeline involving assembly, viral operational taxonomic unit (vOTU) detection and characterization, mapping, and filtering to exclude vOTUs found in negative controls or for which sufficient support for their presence in a given sample was not obtained. The number of blood/fecal shared vOTUs is indicated for all subjects and within the same subject.

(B) Percentage of unique vOTUs shared between fecal and blood within the same subject in patients with CD and healthy subjects. The graph was analyzed for statistical significance using the Mann-Whitney test.

(C) Distribution of predicted bacterial host phyla for the 16 vOTUs shared between fecal and blood samples within the same subject.

(D) Venn diagram illustrating the overlap of Microviridae vOTUs identified in blood and fecal samples across the 29 subjects.

(E) Distribution of predicted bacterial host phyla for the Microviridae vOTUs detected in blood samples from the 29 subjects.

demonstrating that functional phages crossing the epithelial barrier have the potential to reach other tissues via the bloodstream due to the high permeability of the endothelial barrier. This is supported by both our *ex vivo* and *in vivo* data, which show that infectious phages are able to cross the whole intestinal barrier and reach extra-digestive tissues. Although we did not detect phages in peripheral blood, their presence in the liver and spleen of mice suggests technical limitations rather than

absence. The low proportion of positive mice likely reflects this limitation, underscoring the need for improved detection methods and further *in vivo* studies to better characterize translocation kinetics. In addition, phages may also translocate through lymphatic vessels, allowing them to access the lymphatic system, reach the bloodstream, and potentially spread to distant organs.

Using *in vitro* models, we observed that the impairment of epithelial barrier function, a hallmark of Crohn's disease,[2,16,17,25] leads to increased translocation of ΦX174, a member of the Microviridae family. This increase directly correlates with the level of paracellular permeability, emphasizing that Microviridae phage translocation is particularly sensitive to the integrity of the intestinal epithelium. We speculate that phage size may also affect the translocation rate, as ΦX174 is the smallest of the tested phages in this study. Moreover, our virome analysis revealed that patients with Crohn's disease present a higher number of phage sequences shared between fecal and blood samples, suggesting increased gut-to-blood phage translocation.

Although early studies suggested changes in the gut virome in Crohn's disease, recent analyses have not detected a Crohn's disease-specific pattern due to the high variability of the gut virome.[31] Despite such variability, viromes of patients with IBD were found to exacerbate inflammation *in vivo.*[36,57,58] We suggest that the blood phageome may be enriched in Microviridae phages, which are a large community of the gut virome,[26] potentially indicating that they are preferentially translocated from the gut to the blood. Hence, the pattern of phage translocation in patients may contribute to a unique blood viral community, but whether it is involved in Crohn's disease pathogenesis is yet to be determined.

Bacterial translocation has been studied more than viral translocation, with most of the work focusing on microbial DNA or byproducts rather than viable micro-organisms.[20,59–61] For viruses, translocation has been shown by PCR-based detection of parvoviruses in both the gut and serum of necropsied nonhuman primates.[62] In contrast, our virome analysis was designed to specifically detect genomic signals from viral particles rather than free viral DNA. Live intestinal bacteria have been detected in the lamina propria, mesenteric lymph nodes, and liver of murine models with low-grade inflammation or chronic liver disease.[63,64] In the context of acute inflammation, a study reported cultivable *Clostridium innocuum* in mesenteric adipose tissue of both DSS-treated and untreated mice after oral gavage, suggesting that bacterial translocation is not necessarily driven by DSS-induced inflammation.[22] Similarly, our *in vivo* data show that DSS treatment did not increase phage translocation. This aligns with the *in vitro* results demonstrating that pro-inflammatory cytokines have no effect on phage translocation, unlike global disorganization of cell-cell junctions driven by EGTA, which significantly enhances ΦX174 translocation. This suggests that inflammation is not required for phage translocation, which may occur as part of a natural physiological process.

The DSS-induced colitis model in mice could not entirely recapitulate the events observed during human intestinal inflammation via metagenomics, as phage translocation was higher in our cohort of patients with Crohn's disease compared to HSs. Not only does this suggest a more complex, multifactorial basis for the phage translocation process, but it also highlights the need for more representative models to study host-microbiome interactions in IBD.

Another key consideration is the direct impact of phages on human cells, especially concerning their use as therapeutic agents, known as phage therapy. Certain phages have been identified to be highly immunogenic[36,65,66] and to increase endothelial cell permeability,[67] whereas others elicit a minimal immunological response[68,69] and do not trigger pro-inflammatory reactions.[70] Unlike a recent report suggesting that M13 induces a pro-inflammatory response in HT-29 cells,[71] our data show that phages can translocate without compromising epithelial or endothelial barrier function in both physiological and inflammatory contexts. These differences may reflect the inherent divergence between cell lines, as HT-29 and Caco-2/TC7 exhibit distinct epithelial phenotypes, making comparisons challenging. Overall, our findings support the safety of phage therapy. This evidence also strengthens the therapeutic potential of retargeted M13 phages, recently shown to penetrate cancer cells[72] and tumor 3D spheroids.[73] In the context of IBD, we found that only an extremely small fraction of phages can cross the intestinal epithelium, which is a highly selective barrier, suggesting that the effectiveness of phage therapy in the intestinal lumen may not be significantly affected by the translocation rate. The effect of phages on human cells could have important implications for health, but further studies are needed to validate these findings, particularly with intestinal phages.

In conclusion, our study shows that different phages can cross various components of the intestinal barrier, with differences in phage translocation depending on their nature and the integrity of the intestinal barrier. This study supports the potential safety of phages as therapeutic agents, strengthens our understanding of phage dynamics in Crohn's disease, and paves the way for exploring phage translocation in other disorders characterized by increased intestinal permeability.

Limitations of the study

This study has three main limitations. First, experimental validation of phage translocation was performed using three model *E. coli* phages, which do not capture the full diversity of phages present in the intestinal microbiota. Future work should focus on phages directly isolated from the human gut microbiota of both healthy individuals and patients, to investigate their translocation rates and impact on intestinal barrier integrity. Second, the animal experiments were limited to two time points and a single phage dose. Although sufficient to demonstrate phage translocation during intestinal transit, the number of phages recovered from distal organs varied between animals. More, M13 phage enumeration by plaque assay from the liver and spleen of mice did not produce the usual plaque phenotypes, making reliable enumeration impossible. This variability highlights the need for studies with finer kinetic resolution and a broader range of phages and administered doses. Finally, conclusions regarding phage translocation from the gut to the bloodstream in the cohort with Crohn's disease were based on blood and fecal viromes from 29 individuals. These findings should be confirmed in larger cohorts. Moreover, the presence of distinct, functional

viral particles should be proven by viral isolation to confirm the comparative analysis of sequence clusters, since characterizing phage presence by vOTU analysis does not prove the presence of a single phage genome or the presence of functional phages.

RESOURCE AVAILABILITY

Lead contact

Requests for further information and resources should be directed to the lead contact, Luisa De Sordi (luisa.de_sordi@sorbonne-universite.fr).

Materials availability

This study did not generate new unique reagents.

Data and code availability

The sequencing data have been deposited on ENA: PRJNA1126425 and are publicly available. The data and code used to analyze the virome data and generate the related figures have been deposited at Zenodo: https://doi.org/10.5281/zenodo.17433737 and are publicly available as of the date of publication.

ACKNOWLEDGMENTS

We thank Marie-Agnès Petit from the Phage Team at the Micalis Institute, INRAE Jouy-en-Josas, for providing phages and bacterial strains; Juliane Selot from the "TGFb and cancer" team of the CRSA for supplying Cy3 labeled-transferrin; and Dr. Jessica Dahan Saal from Bluets Maternity Hospital (Paris) for the donation of umbilical cords. We also thank Marie-Agnès Petit, Etienne Morel, and Cédric Delevoye for valuable discussion, as well as Raphaëlle Liquard and Lola Savouré for assistance with human cell care and Virginie Puchois Pisano for technical assistance with animal experimentation. We are grateful to Tatiana Ledent and the staff of the animal care facility at the CRSA. We thank the CISA platform at the CRSA for their support, made possible with financial support from Sorbonne Université and from ITMO Cancer of Aviesan and INCa using funds administered by the Institut National de la Santé et de la Recherche Médicale (INSERM). For virome sequencing, we thank M. Monot, L. Ma, and L. Lemée from the Biomics Platform, C2RT, Institut Pasteur, Paris, supported by France Génomique (ANR-10-INBS-09) and IBiSA. BioRender was used to create the figures. This research was supported by grants from the French National Research Agency (ANR), including VENTRIS (no. ANR-21-CE14-0019-01) and PRIMAVERA (no. ANR-19-CE18-0028-01), as well as institutional funding from INSERM, Sorbonne Université, and EPHE-PSL.

AUTHOR CONTRIBUTIONS

Conceptualization, C.D., Q.L.-B., V.C., S.T., and L.D.S.; methodology, C.D., Q.L.-B., I.T., O.S., M.D.P., D.G.-W., V.C., S.T., and L.D.S.; investigation, C.D., I.T., O.S., Y.S., and L.B.; data curation and formal analysis, C.D. and Q.L.-B.; resources, H.S., P.E.C., R.S., A.D., and M.C.; supervision, V.C., S.T., and L.D.S.; funding acquisition, L.D.S. and M.D.P.; writing – original draft, C.D.; writing – review & editing, C.D., Q.L.-B., L.B., A.D., M.C., M.D.P., H.S., D.G.-W., V.C., S.T., and L.D.S.

DECLARATION OF INTERESTS

H.S. declares lecture fees, board membership, or consultancy from Amgen, Fresenius, IPSEN, Actial, Astellas, Danone, THAC, Biose, BiomX, Eligo, Immusmol, Adare, Nestle, Ferring, MSD, Bledina, Pfizer, Biocodex, BMS, Bromatech, Gilead, Janssen, Mayoli, Roche, Sanofi, Servier, Takeda, and AbbVie; has stocks from Enterome Bioscience; and is co-founder of Exeliom Biosciences.

STAR★METHODS

Detailed methods are provided in the online version of this paper and include the following:

- KEY RESOURCES TABLE
- EXPERIMENTAL MODEL AND STUDY PARTICIPANT DETAILS
  - Bacterial strains and phages
  - Cell models
  - Animal experimentation
  - Patients
- METHOD DETAILS
  - Phage preparation
  - Endotoxin removal and determination of the concentration
  - Experimental treatments to increase paracellular permeability in cell models
  - Phage translocation assays in cell models
  - Permeability measurements
  - Cytotoxicity assay and IL-8 secretion
  - Preparation, purification and conjugation of CF488 fluorophore to M13 phages
  - Visualization of the endocytic pathway in HUVECs
  - Confocal microscopy
  - *Ex vivo* assays with Ussing chambers
  - DSS-induced colitis model in mice
  - Quantification of phages by qPCR
  - Sample collection
  - Viral DNA isolation
  - Viral DNA sequencing
  - Determination of vOTUs
  - Characterization of the vOTUs
  - Ecological analysis
- QUANTIFICATION AND STATISTICAL ANALYSIS

SUPPLEMENTAL INFORMATION

Supplemental information can be found online at https://doi.org/10.1016/j.celrep.2025.116726.

Received: September 20, 2024
Revised: August 6, 2025
Accepted: November 21, 2025
Published: December 24, 2025

REFERENCES

1. Le Gall, M., Thenet, S., Aguanno, D., Jarry, A.-C., Genser, L., Ribeiro-Parenti, L., Joly, F., Ledoux, S., Bado, A., and Le Beyec, J. (2019). Intestinal plasticity in response to nutrition and gastrointestinal surgery. Nutr. Rev. *77*, 129–143. https://doi.org/10.1093/nutrit/nuy064.
2. Odenwald, M.A., and Turner, J.R. (2017). The intestinal epithelial barrier: a therapeutic target? Nat. Rev. Gastroenterol. Hepatol. *14*, 9–21. https://doi.org/10.1038/nrgastro.2016.169.
3. Scalise, A.A., Kakogiannos, N., Zanardi, F., Iannelli, F., and Giannotta, M. (2021). The blood–brain and gut–vascular barriers: from the perspective of claudins. Tissue Barriers *9*, 1926190. https://doi.org/10.1080/21688370.2021.1926190.
4. Brescia, P., and Rescigno, M. (2021). The gut vascular barrier: a new player in the gut–liver–brain axis. Trends Mol. Med. *27*, 844–855. https://doi.org/10.1016/j.molmed.2021.06.007.
5. Ilchmann-Diounou, H., and Menard, S. (2020). Psychological Stress, Intestinal Barrier Dysfunctions, and Autoimmune Disorders: An Overview. Front. Immunol. *11*, 1823. https://doi.org/10.3389/fimmu.2020.01823.
6. Tilg, H., Adolph, T.E., and Trauner, M. (2022). Gut-liver axis: Pathophysiological concepts and clinical implications. Cell Metab. *34*, 1700–1718. https://doi.org/10.1016/j.cmet.2022.09.017.

7. König, J., Wells, J., Cani, P.D., García-Ródenas, C.L., MacDonald, T., Mercenier, A., Whyte, J., Troost, F., and Brummer, R.-J. (2016). Human Intestinal Barrier Function in Health and Disease. Clin. Transl. Gastroenterol. *7*, e196. https://doi.org/10.1038/ctg.2016.54.

8. Horowitz, A., Chanez-Paredes, S.D., Haest, X., and Turner, J.R. (2023). Paracellular permeability and tight junction regulation in gut health and disease. Nat. Rev. Gastroenterol. Hepatol. *20*, 417–432. https://doi.org/10.1038/s41575-023-00766-3.

9. Knowles, S.R., Graff, L.A., Wilding, H., Hewitt, C., Keefer, L., and Mikocka-Walus, A. (2018). Quality of Life in Inflammatory Bowel Disease: A Systematic Review and Meta-analyses—Part I. Inflamm. Bowel Dis. *24*, 742–751. https://doi.org/10.1093/ibd/izx100.

10. Knowles, S.R., Keefer, L., Wilding, H., Hewitt, C., Graff, L.A., and Mikocka-Walus, A. (2018). Quality of Life in Inflammatory Bowel Disease: A Systematic Review and Meta-analyses—Part II. Inflamm. Bowel Dis. *24*, 966–976. https://doi.org/10.1093/ibd/izy015.

11. Zhang, Y.-Z., and Li, Y.Y. (2014). Inflammatory bowel disease: Pathogenesis. WJG *20*, 91–99. https://doi.org/10.3748/wjg.v20.i1.91.

12. Borowitz, S.M. (2022). The epidemiology of inflammatory bowel disease: Clues to pathogenesis? Front. Pediatr. *10*, 1103713. https://doi.org/10.3389/fped.2022.1103713.

13. Saez, A., Herrero-Fernandez, B., Gomez-Bris, R., Sánchez-Martinez, H., and Gonzalez-Granado, J.M. (2023). Pathophysiology of Inflammatory Bowel Disease: Innate Immune System. IJMS *24*, 1526. https://doi.org/10.3390/ijms24021526.

14. Hensel, K.O., Boland, V., Postberg, J., Zilbauer, M., Heuschkel, R., Vogel, S., Gödde, D., Wirth, S., and Jenke, A.C. (2014). Differential Expression of Mucosal Trefoil Factors and Mucins in Pediatric Inflammatory Bowel Diseases. Sci. Rep. *4*, 7343. https://doi.org/10.1038/srep07343.

15. Thenet, S., and Carrière, V. (2022). Special Issue on the "Regulation and Physiopathology of the Gut Barrier.". IJMS *23*, 10638. https://doi.org/10.3390/ijms231810638.

16. Turpin, W., Lee, S.-H., Raygoza Garay, J.A., Madsen, K.L., Meddings, J.B., Bedrani, L., Power, N., Espin-Garcia, O., Xu, W., Smith, M.I., et al. (2020). Increased Intestinal Permeability Is Associated With Later Development of Crohn's Disease. Gastroenterology *159*, 2092–2100.e5. https://doi.org/10.1053/j.gastro.2020.08.005.

17. Martini, E., Krug, S.M., Siegmund, B., Neurath, M.F., and Becker, C. (2017). Mend Your Fences. Cell. Mol. Gastroenterol. Hepatol. *4*, 33–46. https://doi.org/10.1016/j.jcmgh.2017.03.007.

18. Cibor, D., Domagala-Rodacka, R., Rodacki, T., Jurczyszyn, A., Mach, T., and Owczarek, D. (2016). Endothelial dysfunction in inflammatory bowel diseases: Pathogenesis, assessment and implications. WJG *22*, 1067–1077. https://doi.org/10.3748/wjg.v22.i3.1067.

19. Jingjie, W., and Jun, S. (2023). Gut vascular barrier in the pathogenesis and resolution of Crohn's disease: A novel link from origination to therapy. Clin. Immunol. *253*, 109683. https://doi.org/10.1016/j.clim.2023.109683.

20. Linares, R., Francés, R., Gutiérrez, A., and Juanola, O. (2021). Bacterial Translocation as Inflammatory Driver in Crohn's Disease. Front. Cell Dev. Biol. *9*, 703310. https://doi.org/10.3389/fcell.2021.703310.

21. Ambrose, N.S., Johnson, M., Burdon, D.W., and Keighley, M.R. (1984). Incidence of pathogenic bacteria from mesenteric lymph nodes and ileal serosa during Crohn's disease surgery. Br. J. Surg. *71*, 623–625. https://doi.org/10.1002/bjs.1800710821.

22. Ha, C.W.Y., Martin, A., Sepich-Poore, G.D., Shi, B., Wang, Y., Gouin, K., Humphrey, G., Sanders, K., Ratnayake, Y., Chan, K.S.L., et al. (2020). Translocation of Viable Gut Microbiota to Mesenteric Adipose Drives Formation of Creeping Fat in Humans. Cell *183*, 666–683.e17. https://doi.org/10.1016/j.cell.2020.09.009.

23. Jin, S., Wetzel, D., and Schirmer, M. (2022). Deciphering mechanisms and implications of bacterial translocation in human health and disease. Curr. Opin. Microbiol. *67*, 102147. https://doi.org/10.1016/j.mib.2022.102147.

24. Luissint, A.-C., Parkos, C.A., and Nusrat, A. (2016). Inflammation and the Intestinal Barrier: Leukocyte–Epithelial Cell Interactions, Cell Junction Remodeling, and Mucosal Repair. Gastroenterology *151*, 616–632. https://doi.org/10.1053/j.gastro.2016.07.008.

25. Di Vincenzo, F., Del Gaudio, A., Petito, V., Lopetuso, L.R., and Scaldaferri, F. (2024). Gut microbiota, intestinal permeability, and systemic inflammation: a narrative review. Intern. Emerg. Med. *19*, 275–293. https://doi.org/10.1007/s11739-023-03374-w.

26. Shkoporov, A.N., and Hill, C. (2019). Bacteriophages of the Human Gut: The "Known Unknown" of the Microbiome. Cell Host Microbe *25*, 195–209. https://doi.org/10.1016/j.chom.2019.01.017.

27. Lourenço, M., De Sordi, L., and Debarbieux, L. (2018). The Diversity of Bacterial Lifestyles Hampers Bacteriophage Tenacity. Viruses *10*, 327. https://doi.org/10.3390/v10060327.

28. Norman, J.M., Handley, S.A., Baldridge, M.T., Droit, L., Liu, C.Y., Keller, B.C., Kambal, A., Monaco, C.L., Zhao, G., Fleshner, P., et al. (2015). Disease-Specific Alterations in the Enteric Virome in Inflammatory Bowel Disease. Cell *160*, 447–460. https://doi.org/10.1016/j.cell.2015.01.002.

29. Clooney, A.G., Sutton, T.D.S., Shkoporov, A.N., Holohan, R.K., Daly, K.M., O'Regan, O., Ryan, F.J., Draper, L.A., Plevy, S.E., Ross, R.P., and Hill, C. (2019). Whole-Virome Analysis Sheds Light on Viral Dark Matter in Inflammatory Bowel Disease. Cell Host Microbe *26*, 764–778.e5. https://doi.org/10.1016/j.chom.2019.10.009.

30. Lepage, P., Colombet, J., Marteau, P., Sime-Ngando, T., Doré, J., and Leclerc, M. (2008). Dysbiosis in inflammatory bowel disease: a role for bacteriophages? Gut *57*, 424–425. https://doi.org/10.1136/gut.2007.134668.

31. Stockdale, S.R., Shkoporov, A.N., Khokhlova, E.V., Daly, K.M., McDonnell, S.A., O' Regan, O., Nolan, J.A., Sutton, T.D.S., Clooney, A.G., Ryan, F.J., et al. (2023). Interpersonal variability of the human gut virome confounds disease signal detection in IBD. Commun. Biol. *6*, 221. https://doi.org/10.1038/s42003-023-04592-w.

32. Lamy-Besnier, Q., Theodorou, I., Billaud, M., Zhang, H., Brot, L., Culot, A., Abriat, G., Sokol, H., De Paepe, M., Petit, M.-A., and De Sordi, L. (2024). The human blood harbors a phageome which differs in Crohn's disease. Preprint at bioRxiv. https://doi.org/10.1101/2024.06.04.597176.

33. Bichet, M.C., Chin, W.H., Richards, W., Lin, Y.-W., Avellaneda-Franco, L., Hernandez, C.A., Oddo, A., Chernyavskiy, O., Hilsenstein, V., Neild, A., et al. (2021). Bacteriophage uptake by mammalian cell layers represents a potential sink that may impact phage therapy. iScience *24*, 102287. https://doi.org/10.1016/j.isci.2021.102287.

34. Le, H.T., Lubian, A.F., Bowring, B., Van Der Poorten, D., Iredell, J., George, J., Venturini, C., Ahlenstiel, G., and Read, S. (2024). Using a human colonoid-derived monolayer to study bacteriophage translocation. Gut Microbes *16*, 2331520. https://doi.org/10.1080/19490976.2024.2331520.

35. Nguyen, S., Baker, K., Padman, B.S., Patwa, R., Dunstan, R.A., Weston, T.A., Schlosser, K., Bailey, B., Lithgow, T., Lazarou, M., et al. (2017). Bacteriophage Transcytosis Provides a Mechanism To Cross Epithelial Cell Layers. mBio *8*, e01874-17. https://doi.org/10.1128/mBio.01874-17.

36. Gogokhia, L., Buhrke, K., Bell, R., Hoffman, B., Brown, D.G., Hanke-Gogokhia, C., Ajami, N.J., Wong, M.C., Ghazaryan, A., Valentine, J.F., et al. (2019). Expansion of Bacteriophages Is Linked to Aggravated Intestinal Inflammation and Colitis. Cell Host Microbe *25*, 285–299.e8. https://doi.org/10.1016/j.chom.2019.01.008.

37. Adiliaghdam, F., Amatullah, H., Digumarthi, S., Saunders, T.L., Rahman, R.-U., Wong, L.P., Sadreyev, R., Droit, L., Paquette, J., Goyette, P., et al. (2022). Human enteric viruses autonomously shape inflammatory bowel disease phenotype through divergent innate immunomodulation. Sci. Immunol. *7*, eabn6660. https://doi.org/10.1126/sciimmunol.abn6660.

38. Lehti, T.A., Pajunen, M.I., Skog, M.S., and Finne, J. (2017). Internalization of a polysialic acid-binding Escherichia coli bacteriophage into eukaryotic neuroblastoma cells. Nat. Commun. *8*, 1915. https://doi.org/10.1038/s41467-017-02057-3.

39. Pinto, M., Robine-Leon, S., Appay, M.-D., Kedinger, M., Triadou, N., Dussaulx, E., Lacroix, B., Simon-Assmann, P., Haffen, K., Fogh, J., et al. (1983). Enterocyte-like differentiation and polarization of the human colon carcinoma cell line Caco-2 in culture. Biol. Cell *47*, 323–330. https://inserm.hal.science/inserm-04076258v1.

40. Chantret, I., Rodolosse, A., Barbat, A., Dussaulx, E., Brot-Laroche, E., Zweibaum, A., and Rousset, M. (1994). Differential expression of sucrase-isomaltase in clones isolated from early and late passages of the cell line caco-2: Evidence for glucose-dependent negative regulation. J. Cell Sci. *107*, 213–225. https://doi.org/10.1242/jcs.107.1.213.

41. Kawabata, H. (2019). Transferrin and transferrin receptors update. Free Radic. Biol. Med. *133*, 46–54. https://doi.org/10.1016/j.freeradbiomed.2018.06.037.

42. Nejdfors, P., Ekelund, M., Jeppsson, B., and Weström, B.R. (2000). Mucosal in Vitro Permeability in the Intestinal Tract of the Pig, the Rat, and Man: Species- and Region-Related Differences. Scand. J. Gastroenterol. *35*, 501–507. https://doi.org/10.1080/003655200750023769.

43. Petit, C.S.V., Barreau, F., Besnier, L., Gandille, P., Riveau, B., Chateau, D., Roy, M., Berrebi, D., Svrcek, M., Cardot, P., et al. (2012). Requirement of Cellular Prion Protein for Intestinal Barrier Function and Mislocalization in Patients With Inflammatory Bowel Disease. Gastroenterology *143*, 122–132.e15. https://doi.org/10.1053/j.gastro.2012.03.029.

44. Camilleri, M. (2021). Human Intestinal Barrier: Effects of Stressors, Diet, Prebiotics, and Probiotics. Clin. Transl. Gastroenterol. *12*, e00308. https://doi.org/10.14309/ctg.0000000000000308.

45. García-Gamboa, R., Díaz-Torres, O., Senés-Guerrero, C., Gradilla-Hernández, M.S., Moya, A., Pérez-Brocal, V., Garcia-Gonzalez, A., and González-Avila, M. (2024). Associations between bacterial and fungal communities in the human gut microbiota and their implications for nutritional status and body weigh t. Sci. Rep. *14*, 5703. https://doi.org/10.1038/s41598-024-54782-7.

46. Sanmukh, S.G., Santos, N.J., Barquilha, C.N., Dos Santos, S.A.A., Duran, B.O.S., Delella, F.K., Moroz, A., Justulin, L.A., Carvalho, H.F., and Felisbino, S.L. (2021). Exposure to Bacteriophages T4 and M13 Increases Integrin Gene Expression and Impairs Migration of Human PC-3 Prostate Cancer Cells. Antibiotics *10*, 1202. https://doi.org/10.3390/antibiotics10101202.

47. Fievez, V., Plapied, L., Plaideau, C., Legendre, D., Des Rieux, A., Pourcelle, V., Freichels, H., Jérôme, C., Marchand, J., Préat, V., and Schneider, Y.J. (2010). In vitro identification of targeting ligands of human M cells by phage display. Int. J. Pharm. *394*, 35–42. https://doi.org/10.1016/j.ijpharm.2010.04.023.

48. Wang, R., Li, H.-D., Cao, Y., Wang, Z.-Y., Yang, T., and Wang, J.-H. (2023). M13 phage: a versatile building block for a highly specific analysis platform. Anal. Bioanal. Chem. *415*, 3927–3944. https://doi.org/10.1007/s00216-023-04606-w.

49. Tian, Y., Wu, M., Liu, X., Liu, Z., Zhou, Q., Niu, Z., and Huang, Y. (2015). Probing the Endocytic Pathways of the Filamentous Bacteriophage in Live Cells Using Ratiometric pH Fluorescent Indicator. Adv. Healthc. Mater. *4*, 413–419. https://doi.org/10.1002/adhm.201400508.

50. Spadoni, I., Zagato, E., Bertocchi, A., Paolinelli, R., Hot, E., Di Sabatino, A., Caprioli, F., Bottiglieri, L., Oldani, A., Viale, G., et al. (2015). A gut-vascular barrier controls the systemic dissemination of bacteria. Science *350*, 830–834. https://doi.org/10.1126/science.aad0135.

51. He, S., Guo, Y., Zhao, J., Xu, X., Wang, N., and Liu, Q. (2020). Ferulic Acid Ameliorates Lipopolysaccharide-Induced Barrier Dysfunction via MicroRNA-200c-3p-Mediated Activation of PI3K/AKT Pathway in Caco-2 Cells. Front. Pharmacol. *11*, 376. https://doi.org/10.3389/fphar.2020.00376.

52. Ghezzal, S., Postal, B.G., Quevrain, E., Brot, L., Seksik, P., Leturque, A., Thenet, S., and Carrière, V. (2020). Palmitic acid damages gut epithelium integrity and initiates inflammatory cytokine production. Biochim. Biophys. Acta. Mol. Cell Biol. Lipids *1865*, 158530. https://doi.org/10.1016/j.bbalip.2019.158530.

53. Kan, L., and Barr, J.J. (2023). A Mammalian Cell's Guide on How to Process a Bacteriophage. Annu. Rev. Virol. *10*, 183–198. https://doi.org/10.1146/annurev-virology-111821-111322.

54. Hamzeh-Mivehroud, M., Mahmoudpour, A., Rezazadeh, H., and Dastmalchi, S. (2008). Non-specific translocation of peptide-displaying bacteriophage particles across the gastrointestinal barrier. Eur. J. Pharm. Biopharm. *70*, 577–581. https://doi.org/10.1016/j.ejpb.2008.06.005.

55. Keller, R., and Engley, F.B. (1958). Fate of bacteriophage particles introduced into mice by various routes. Proc. Soc. Exp. Biol. Med. *98*, 577–580. https://doi.org/10.3181/00379727-98-24112.

56. Dąbrowska, K. (2019). Phage therapy: What factors shape phage pharmacokinetics and bioavailability? Systematic and critical review. Med. Res. Rev. *39*, 2000–2025. https://doi.org/10.1002/med.21572.

57. Cao, Z., Fan, D., Sun, Y., Huang, Z., Li, Y., Su, R., Zhang, F., Li, Q., Yang, H., Zhang, F., et al. (2024). The gut ileal mucosal virome is disturbed in patients with Crohn's disease and exacerbates intestinal inflammation in mice. Nat. Commun. *15*, 1638. https://doi.org/10.1038/s41467-024-45794-y.

58. Sinha, A., Li, Y., Mirzaei, M.K., Shamash, M., Samadfam, R., King, I.L., and Maurice, C.F. (2022). Transplantation of bacteriophages from ulcerative colitis patients shifts the gut bacteriome and exacerbates the severity of DSS colitis. Microbiome *10*, 105. https://doi.org/10.1186/s40168-022-01275-2.

59. Vrakas, S., Mountzouris, K.C., Michalopoulos, G., Karamanolis, G., Papatheodoridis, G., Tzathas, C., and Gazouli, M. (2017). Intestinal Bacteria Composition and Translocation of Bacteria in Inflammatory Bowel Disease. PLoS One *12*, e0170034. https://doi.org/10.1371/journal.pone.0170034.

60. Kosovac, K., Brenmoehl, J., Holler, E., Falk, W., Schoelmerich, J., Hausmann, M., and Rogler, G. (2010). Association of the NOD2 genotype with bacterial translocation via altered cell–cell contacts in Crohn's disease patients. Inflamm. Bowel Dis. *16*, 1311–1321. https://doi.org/10.1002/ibd.21223.

61. O'Brien, C.L., Pavli, P., Gordon, D.M., and Allison, G.E. (2014). Detection of bacterial DNA in lymph nodes of Crohn's disease patients using high throughput sequencing. Gut *63*, 1596–1606. https://doi.org/10.1136/gutjnl-2013-305320.

62. Handley, S.A., Thackray, L.B., Zhao, G., Presti, R., Miller, A.D., Droit, L., Abbink, P., Maxfield, L.F., Kambal, A., Duan, E., et al. (2012). Pathogenic Simian Immunodeficiency Virus Infection Is Associated with Expansion of the Enteric Virome. Cell *151*, 253–266. https://doi.org/10.1016/j.cell.2012.09.024.

63. Amar, J., Chabo, C., Waget, A., Klopp, P., Vachoux, C., Bermúdez-Humarán, L.G., Smirnova, N., Bergé, M., Sulpice, T., Lahtinen, S., et al. (2011). Intestinal mucosal adherence and translocation of commensal bacteria at the early onset of type 2 diabetes: molecular mechanisms and probiotic treatment. EMBO Mol. Med. *3*, 559–572. https://doi.org/10.1002/emmm.201100159.

64. Llorente, C., Jepsen, P., Inamine, T., Wang, L., Bluemel, S., Wang, H.J., Loomba, R., Bajaj, J.S., Schubert, M.L., Sikaroodi, M., et al. (2017). Gastric acid suppression promotes alcoholic liver disease by inducing overgrowth of intestinal Enterococcus. Nat. Commun. *8*, 837. https://doi.org/10.1038/s41467-017-00796-x.

65. Fluckiger, A., Daillère, R., Sassi, M., Sixt, B.S., Liu, P., Loos, F., Richard, C., Rabu, C., Alou, M.T., Goubet, A.-G., et al. (2020). Cross-reactivity between tumor MHC class I–restricted antigens and an enterococcal bacteriophage. Science *369*, 936–942. https://doi.org/10.1126/science.aax0701.

66. Sweere, J.M., Van Belleghem, J.D., Ishak, H., Bach, M.S., Popescu, M., Sunkari, V., Kaber, G., Manasherob, R., Suh, G.A., Cao, X., et al. (2019). Bacteriophage trigger antiviral immunity and prevent clearance of bacterial infection. Science *363*, eaat9691. https://doi.org/10.1126/science.aat9691.

67. Møller-Olsen, C., Ross, T., Leppard, K.N., Foisor, V., Smith, C., Grammatopoulos, D.K., and Sagona, A.P. (2020). Bacteriophage K1F targets Escherichia coli K1 in cerebral endothelial cells and influences the barrier function. Sci. Rep. *10*, 8903. https://doi.org/10.1038/s41598-020-65867-4.

68. Federici, S., Kredo-Russo, S., Valdés-Mas, R., Kviatcovsky, D., Weinstock, E., Matiuhin, Y., Silberberg, Y., Atarashi, K., Furuichi, M., Oka, A., et al. (2022). Targeted suppression of human IBD-associated gut microbiota commensals by phage consortia for treatment of intestinal inflammation. Cell *185*, 2879–2898.e24. https://doi.org/10.1016/j.cell.2022.07.003.

69. Petrovic Fabijan, A., Lin, R.C.Y., Ho, J., Maddocks, S., Ben Zakour, N.L., Iredell, J.R., Westmead Bacteriophage Therapy Team; Khalid, A., Venturini, C., Chard, R., et al. (2020). Safety of bacteriophage therapy in severe Staphylococcus aureus infection. Nat. Microbiol. *5*, 465–472. https://doi.org/10.1038/s41564-019-0634-z.

70. Bichet, M.C., Adderley, J., Avellaneda-Franco, L., Magnin-Bougma, I., Torriero-Smith, N., Gearing, L.J., Deffrasnes, C., David, C., Pepin, G., Gantier, M.P., et al. (2023). Mammalian cells internalize bacteriophages and use them as a resource to enhance cellular growth and survival. PLoS Biol. *21*, e3002341. https://doi.org/10.1371/journal.pbio.3002341.

71. Varadan, A.C., and Grasis, J.A. (2025). Filamentous bacteriophage M13 induces proinflammatory responses in intestinal epithelial cells. Infect. Immun. *93*, e00618-24. https://doi.org/10.1128/iai.00618-24.

72. Ulfo, L., Cantelli, A., Petrosino, A., Costantini, P.E., Nigro, M., Starinieri, F., Turrini, E., Zadran, S.K., Zuccheri, G., Saporetti, R., et al. (2022). Orthogonal nanoarchitectonics of M13 phage for receptor targeted anticancer photodynamic therapy. Nanoscale *14*, 632–641. https://doi.org/10.1039/d1nr06053h.

73. Turrini, E., Ulfo, L., Costantini, P.E., Saporetti, R., Di Giosia, M., Nigro, M., Petrosino, A., Pappagallo, L., Kaltenbrunner, A., Cantelli, A., et al. (2024). Molecular engineering of a spheroid-penetrating phage nanovector for photodynamic treatment of colon cancer cells. Cell. Mol. Life Sci. *81*, 144. https://doi.org/10.1007/s00018-024-05174-7.

74. De Paepe, M., De Monte, S., Robert, L., Lindner, A.B., and Taddei, F. (2010). Emergence of Variability in Isogenic Escherichia coli Populations Infected by a Filamentous Virus. PLoS One *5*, e11823. https://doi.org/10.1371/journal.pone.0011823.

75. Bushnell, B. (2014). BBMap: A Fast, Accurate, Splice-Aware Aligner (Lawrence Berkeley National Laboratory). https://escholarship.org/uc/item/1h3515gn.

76. Kent, W.J. (2002). BLAT —The BLAST -Like Alignment Tool. Genome Res. *12*, 656–664. https://doi.org/10.1101/gr.229202.

77. Langmead, B., and Salzberg, S.L. (2012). Fast gapped-read alignment with Bowtie 2. Nat. Methods *9*, 357–359. https://doi.org/10.1038/nmeth.1923.

78. Vasimuddin, M., Misra, S., Li, H., and Aluru, S. (2019). Efficient Architecture-Aware Acceleration of BWA-MEM for Multicore Systems. In 2019 IEEE International Parallel and Distributed Processing Symposium (IPDPS) (IEEE), pp. 314–324. https://doi.org/10.1109/IPDPS.2019.00041.

79. Nayfach, S., Camargo, A.P., Schulz, F., Eloe-Fadrosh, E., Roux, S., and Kyrpides, N.C. (2021). CheckV assesses the quality and completeness of metagenome-assembled viral genomes. Nat. Biotechnol. *39*, 578–585. https://doi.org/10.1038/s41587-020-00774-7.

80. Chen, S., Zhou, Y., Chen, Y., and Gu, J. (2018). fastp: an ultra-fast all-in-one FASTQ preprocessor. Bioinformatics *34*, i884–i890. https://doi.org/10.1093/bioinformatics/bty560.

81. Pandolfo, M., Telatin, A., Lazzari, G., Adriaenssens, E.M., and Vitulo, N. (2022). MetaPhage: an Automated Pipeline for Analyzing, Annotating, and Classifying Bacteriophages in Metagenomics Sequencing Data. mSystems *7*, e00741-22. https://doi.org/10.1128/msystems.00741-22.

82. Roux, S., Camargo, A.P., Coutinho, F.H., Dabdoub, S.M., Dutilh, B.E., Nayfach, S., and Tritt, A. (2023). iPHoP: An integrated machine learning framework to maximize host prediction for metagenome-derived viruses of archaea and bacteria. PLoS Biol. *21*, e3002083. https://doi.org/10.1371/journal.pbio.3002083.

83. McMurdie, P.J., and Holmes, S. (2013). phyloseq: An R Package for Reproducible Interactive Analysis and Graphics of Microbiome Census Data. PLoS One *8*, e61217. https://doi.org/10.1371/journal.pone.0061217.

84. Li, H., Handsaker, B., Wysoker, A., Fennell, T., Ruan, J., Homer, N., Marth, G., Abecasis, G., and Durbin, R.; 1000 Genome Project Data Processing Subgroup (2009). The Sequence Alignment/Map format and SAMtools. Bioinformatics *25*, 2078–2079. https://doi.org/10.1093/bioinformatics/btp352.

85. Prjibelski, A., Antipov, D., Meleshko, D., Lapidus, A., and Korobeynikov, A. (2020). Using SPAdes De Novo Assembler. CP Bioinformatics *70*, e102. https://doi.org/10.1002/cpbi.102.

86. Bin Jang, H., Bolduc, B., Zablocki, O., Kuhn, J.H., Roux, S., Adriaenssens, E.M., Brister, J.R., Kropinski, A.M., Krupovic, M., Lavigne, R., et al. (2019). Taxonomic assignment of uncultivated prokaryotic virus genomes is enabled by gene-sharing networks. Nat. Biotechnol. *37*, 632–639. https://doi.org/10.1038/s41587-019-0100-8.

87. Kieft, K., Zhou, Z., and Anantharaman, K. (2020). VIBRANT: automated recovery, annotation and curation of microbial viruses, and evaluation of viral community function from genomic sequences. Microbiome *8*, 90. https://doi.org/10.1186/s40168-020-00867-0.

88. Guo, J., Bolduc, B., Zayed, A.A., Varsani, A., Dominguez-Huerta, G., Delmont, T.O., Pratama, A.A., Gazitúa, M.C., Vik, D., Sullivan, M.B., and Roux, S. (2021). VirSorter2: a multi-classifier, expert-guided approach to detect diverse DNA and RNA viruses. Microbiome *9*, 37. https://doi.org/10.1186/s40168-020-00990-y.

89. Blattner, F.R., Plunkett, G., Bloch, C.A., Perna, N.T., Burland, V., Riley, M., Collado-Vides, J., Glasner, J.D., Rode, C.K., Mayhew, G.F., et al. (1997). The Complete Genome Sequence of *Escherichia coli* K-12. Science *277*, 1453–1462. https://doi.org/10.1126/science.277.5331.1453.

90. Aguanno, D., Coquant, G., Postal, B.G., Osinski, C., Wieckowski, M., Stockholm, D., Grill, J.-P., Carrière, V., Seksik, P., and Thenet, S. (2020). The intestinal quorum sensing 3-oxo-C12:2 Acyl homoserine lactone limits cytokine-induced tight junction disruption. Tissue Barriers *8*, 1832877. https://doi.org/10.1080/21688370.2020.1832877.

91. Postal, B.G., Aguanno, D., Thenet, S., and Carrière, V. (2021). Rapid Evaluation of Intestinal Paracellular Permeability Using the Human Enterocytic-Like Caco-2/TC7 Cell Line. In Permeability Barrier Methods in Molecular Biology, K. Turksen, ed. (Springer US), pp. 13–26. https://doi.org/10.1007/7651_2021_366.

92. Petrosino, A., Saporetti, R., Starinieri, F., Sarti, E., Ulfo, L., Boselli, L., Cantelli, A., Morini, A., Zadran, S.K., Zuccheri, G., et al. (2023). A modular phage vector platform for targeted photodynamic therapy of Gram-negative bacterial pathogens. iScience *26*, 108032. https://doi.org/10.1016/j.isci.2023.108032.

93. Passaretti, P., Khan, I., Dafforn, T.R., and Goldberg Oppenheimer, P. (2020). Improvements in the production of purified M13 bacteriophage bio-nanoparticle. Sci. Rep. *10*, 18538. https://doi.org/10.1038/s41598-020-75205-3.

94. Aguanno, D., Postal, B.G., Carrière, V., and Thenet, S. (2021). Use of Ussing Chambers to Measure Paracellular Permeability to Macromolecules in Mouse Intestine. In Permeability Barrier Methods in Molecular Biology, K. Turksen, ed. (Springer US), pp. 1–11. https://doi.org/10.1007/7651_2021_367.

95. Lourenço, M., Chaffringeon, L., Lamy-Besnier, Q., Pédron, T., Campagne, P., Eberl, C., Bérard, M., Stecher, B., Debarbieux, L., and De Sordi, L. (2020). The Spatial Heterogeneity of the Gut Limits Predation and Fosters Coex istence of Bacteria and Bacteriophages. Cell Host Microbe *28*, 390–401.e5. https://doi.org/10.1016/j.chom.2020.06.002.

96. Peng, X., Nguyen, A., and Ghosh, D. (2018). Quantification of M13 and T7 bacteriophages by TaqMan and SYBR green qPCR. J. Virol. Methods *252*, 100–107. https://doi.org/10.1016/j.jviromet.2017.11.012.

97. Billaud, M., Lamy-Besnier, Q., Lossouarn, J., Moncaut, E., Dion, M.B., Moineau, S., Traoré, F., Le Chatelier, E., Denis, C., Estelle, J., et al. (2021). Analysis of viromes and microbiomes from pig fecal samples reveals that phages and prophages rarely carry antibiotic resistance genes. ISME Commun. *1*, 55. https://doi.org/10.1038/s43705-021-00054-8.

98. Trubl, G., Roux, S., Solonenko, N., Li, Y.-F., Bolduc, B., Rodríguez-Ramos, J., Eloe-Fadrosh, E.A., Rich, V.I., and Sullivan, M.B. (2019). Towards optimized viral metagenomes for double-stranded and single-stranded DNA viruses from challenging soils. PeerJ *7*, e7265. https://doi.org/10.7717/peerj.7265.

99. Shah, S.A., Deng, L., Thorsen, J., Pedersen, A.G., Dion, M.B., Castro-Mejía, J.L., Silins, R., Romme, F.O., Sausset, R., Jessen, L.E., et al. (2023). Expanding known viral diversity in the healthy infant gut. Nat. Microbiol. *8*, 986–998. https://doi.org/10.1038/s41564-023-01345-7.

100. Camarillo-Guerrero, L.F., Almeida, A., Rangel-Pineros, G., Finn, R.D., and Lawley, T.D. (2021). Massive expansion of human gut bacteriophage diversity. Cell *184*, 1098–1109.e9. https://doi.org/10.1016/j.cell.2021.01.029.

101. Gregory, A.C., Zablocki, O., Zayed, A.A., Howell, A., Bolduc, B., and Sullivan, M.B. (2020). The Gut Virome Database Reveals Age-Dependent Patterns of Virome Diversity in the Human Gut. Cell Host Microbe *28*, 724–740.e8. https://doi.org/10.1016/j.chom.2020.08.003.

102. Nayfach, S., Páez-Espino, D., Call, L., Low, S.J., Sberro, H., Ivanova, N.N., Proal, A.D., Fischbach, M.A., Bhatt, A.S., Hugenholtz, P., and Kyrpides, N.C. (2021). Metagenomic compendium of 189,680 DNA viruses from the human gut microbiome. Nat. Microbiol. *6*, 960–970. https://doi.org/10.1038/s41564-021-00928-6.

103. Tisza, M.J., and Buck, C.B. (2021). A catalog of tens of thousands of viruses from human metagenomes reveals hidden associations with chronic diseases. Proc. Natl. Acad. Sci. USA *118*, e2023202118. https://doi.org/10.1073/pnas.2023202118.

104. O'Leary, N.A., Wright, M.W., Brister, J.R., Ciufo, S., Haddad, D., McVeigh, R., Rajput, B., Robbertse, B., Smith-White, B., Ako-Adjei, D., et al. (2016). Reference sequence (RefSeq) database at NCBI: current status, taxonomic expansion, and functional annotation. Nucleic Acids Res. *44*, D733–D745. https://doi.org/10.1093/nar/gkv1189.

105. Cook, R., Brown, N., Redgwell, T., Rihtman, B., Barnes, M., Clokie, M., Stekel, D.J., Hobman, J., Jones, M.A., and Millard, A. (2021). INfrastructure for a PHAge REference Database: Identification of Large-Scale Biases in the Current Collection of Cultured Phage Genomes. PHAGE *2*, 214–223. https://doi.org/10.1089/phage.2021.0007.

STAR★METHODS

KEY RESOURCES TABLE

REAGENT or RESOURCE	SOURCE	IDENTIFIER
Antibodies		
Anti-rabbit Tricellulin (MARVELD2) antibody	Thermo Fisher Scientific	Cat# 700191; RRID: AB_2532298
Anti-mouse E-cadherin antibody	Takara Bio Europe	Cat# M108; RRID: AB_2895157
Anti-mouse IgG (Alexa Fluor 647)	Invitrogen, Thermo Fisher Scientific	Cat# A31571; RRID: AB_162542
Anti-mouse ZO-1 antibody	Thermo Fisher Scientific	Cat# 33–9100; RRID: AB_2533147
Anti-rabbit IgG (Alexa Fluor 546)	Invitrogen, Thermo Fisher Scientific	Cat# A11010; RRID:AB_2534077
Bacterial and virus strains		
Escherichia coli C+	ATCC	Cat#: 8739
Escherichia coli K-12 MG1655	ATCC	Cat#: 700926
Escherichia coli K-12 MG1655 F+	De Paepe et al.[74]	N/A
M13yfp phage	De Paepe et al.[74]	N/A
T4 phage	Stock laboratory	GenBank: AF158101.6
ΦX174 phage	Stock laboratory	GenBank: J02482.1
Biological samples		
Human stools	Saint-Antoine Hospital	IRB 00003835
Human whole blood	Saint-Antoine Hospital	IRB 00003835
Chemicals, peptides, and recombinant proteins		
Benzonase-nuclease	Sigma-Aldrich	Cat#: E1014-5KU
Bovine Serum Albumin (BSA)	Sigma-Aldrich	Cat#: A2153
CF™ 488A succinimidyl ester	Biotium	Cat#: CF488-SE
Chloroform	VWR Chemicals	Cat# 22711.290
Chloroform:Isoamyl alcohol 24:1	Sigma-Aldrich	Cat#: C0549-1QT
Cy™3 ChromPure® Human Transferrin	Jackson ImmunoResearch	Cat# 009-160-050; RRID: AB_2337082
DAPI	Invitrogen, Thermo Fisher Scientific	Cat#: D1306
Dextran Sulfate Sodium (DSS)	MP Biomedicals	Cat#: 02160110-CF
DMEM (1×) + GlutaMAX™	Gibco, Thermo Fisher Scientific	Cat#: 61965026
DNase (2 U/μL) TURBO™	Invitrogen, Thermo Fisher Scientific	Cat#: AM2238
EBM-2 Endothelial Cell Basal Medium-2	Lonza	Cat#: CC-3156
EDTA	Sigma-Aldrich	Cat#: E5391
EGM-2 Endothelial Cell Growth Medium-2 BulletKit™	Lonza	Cat#: CC-3162
EGTA	Sigma-Aldrich	Cat#: E4378
Fetal Calf Serum	Sigma-Aldrich	Cat#: F7524
FITC-Dextran 4 kDa (FD4)	TdB Labs	Cat#: 60842-46-8
Human fibronectin	Sigma-Aldrich	Cat#: 341635
Kanamycin	Sigma-Aldrich	Cat#: K4000
LB Broth	Sigma-Aldrich	Cat#: L30022
Lysotracker® Deep Red	Thermo Fisher Scientific	Cat#: L12492
MEM Non-Essential Amino Acids Solution (100×)	Gibco, Thermo Fisher Scientific	Cat#: 11140035
Paraformaldehyde (PFA) 16%	Thermo Fisher Scientific	Cat#: 043368.9M
Penicillin-Streptomycin (10,000 U/mL)	Gibco, Thermo Fisher Scientific	Cat#: 1514022
Phalloïdin (Alexa Fluor 647 or 546)	Invitrogen, Thermo Fisher Scientific	Cat#: A22287 or A22283
Phenol:Chloroform:Isoamyl Alcohol 25: 24:1	Sigma-Aldrich	Cat#: P3803-400ML

(*Continued on next page*)

Continued

REAGENT or RESOURCE	SOURCE	IDENTIFIER
Pierce™ high-capacity endotoxin removal resin	Thermo Fisher Scientific	Cat#: 88270
Power SYBR™ Green PCR Master Mix	Applied Biosystems, Fisher Scientific	Cat#: 10658255
ProLong™ Gold Antifade Mountant	Invitrogen, Thermo Fisher Scientific	Cat#: P36934
Proteinase K	Thermo Fisher Scientific	Cat#: EO0491
Recombinant human interferon-γ (IFNγ)	Bio-Techne	Cat#: 285-IF/CF
Recombinant human tumor necrosis factor-α (TNFα)	Bio-Techne	Cat#: 210-TA/CF
RNA later	Sigma-Aldrich	Cat#: R0901
RNase I (10 U/μL)	Thermo Scientific	Cat#: EN0601
Triton X-100	Sigma-Aldrich	Cat#: T9284
Critical commercial assays		
Cytotoxicity Detection KitPLUS (LDH)	Roche	Cat#: 04744926001
Duoset human IL-8 ELISA kit	R&D Systems	Cat#: DY208
EndoTrap® HD kit	Lionex	Cat#: LET0010
Pierce™ Chromogenic Endotoxin Quant kit	Thermo Fisher Scientific	Cat#: A39552S
xGen™ DNA Library Preparation kit	Integrated DNA Technologies	Cat#: 10009821
Deposited data		
Metagenomic data	ENA	PRJNA1126425
vOTU annotation	entrepot.recherche.data.gouv.fr	https://doi.org/10.57745/FTIXS5
Experimental models: Cell lines		
Caco-2/TC7 human colon adenocarcinoma cell line	stock laboratory	Chantret et al.[40]
HUVEC primary endothelial cells	Lonza	Cat#: C2519A
HUVEC primary endothelial cells	Stock laboratory prepared from umbilical cords donated by Bluets Maternity Hospital (Paris)	MTA Sorbonne Université C22/1604
Experimental models: Organisms/strains		
Mouse: C57BL/6J	Charles River	Cat#: 000664, RRID: IMSR_JAX:000664
Oligonucleotides		
M13 phage; Forward CACCGTTCATCTGTCCTCTTT; Reverse CGACCTGCTCCATGTTACTTAG	Eurogentec	N/A
T4 phage; Forward ACTGGCCAGGTATTCGCA; Reverse ATGCTTCTTTAGCAGCGGCA	Eurogentec	N/A
ΦX174 phage; Forward GGTTCGTCAAGGACTGGTT; Reverse TTGAACAGCATCGGACTCAG	Eurogentec	N/A
Software and algorithms		
bbmap 38.86	Bushnell[75]	https://github.com/BioInfoTools/BBMap
Biorender	Biorender	https://www.biorender.com/
BLAT 36	Kent[76]	https://github.com/djhshih/blat
Bowtie2 2.4.1	Langmead and Salzberg[77]	https://github.com/BenLangmead/bowtie2
bwa-mem2 2.2.1	Vasimuddin et al.[78]	https://github.com/bwa-mem2/bwa-mem2
CheckV 0.8.1	Nayfach et al.[79]	https://bitbucket.org/berkeleylab/checkv
fastp 0.23.1	Chen et al.[80]	https://github.com/OpenGene/fastp
graphanalyzer 1.5.1	Pandolfo et al.[81]	https://github.com/lazzarigioele/graphanalyzer
GraphPad Prism	GraphPad Software	https://www.graphpad.com/
ImageJ Fiji	NIH	https://imagej.nih.gov/ij/
iPHoP 1.2.0	Roux et al.[82]	https://bitbucket.org/srouxjgi/iphop

(*Continued on next page*)

Continued

REAGENT or RESOURCE	SOURCE	IDENTIFIER
msamtools 1.1.3.	Arumugam Lab	https://github.com/arumugamlab/msamtools
QuPath	QuPath	https://qupath.github.io/
R package phyloseq 1.46.0.	McMurdie and Holmes[83]	https://www.bioconductor.org/packages/release/bioc/html/phyloseq.html
Samtools 1.9	Li et al.[84]	https://www.htslib.org/
SPAdes 3.14.0	Bankevich et al.[85]	https://github.com/ablab/spades
vContact2 0.9.19	Jang et al.[86]	https://bitbucket.org/MAVERICLab/vcontact2
VIBRANT 1.2.1	Kieft et al.[87]	https://github.com/AnantharamanLab/VIBRANT
VirSorter2 2.2.3	Guo et al.[88]	https://github.com/jiarong/VirSorter2

EXPERIMENTAL MODEL AND STUDY PARTICIPANT DETAILS

Bacterial strains and phages

The bacterial strains used in this study, *Escherichia coli* K-12 MG1655 F+,[74] *Escherichia coli* K-12 MG1655,[89] and *Escherichia coli* C+ (ATCC 8739) were cultured in Luria-Bertani (LB) media (10 g/L tryptone, 5 g/L yeast extract, 5 g/L NaCl) at 37°C with shaking overnight and used to amplify M13yfp,[74] T4 and ΦX174 phages, respectively, which were titered by plaque assay (Table 1).

Cell models

The Caco-2/TC7 cell line is a clonal population of human colon carcinoma-derived Caco-2 cells.[39,40] Caco-2/TC7 cells were cultured on six-well Transwell 3 μm-pore size filters (Sarstedt) for 19 days to obtain fully differentiated enterocyte-like cells as previously described.[90] Briefly, cells were cultured in high-glucose Dulbecco's modified Eagle's medium Glutamax (Thermo Fisher Scientific) supplemented with 20% heat-inactivated fetal calf serum (FCS) (Sigma-Aldrich), 1% non-essential amino acids, penicillin (100 IU/mL), and streptomycin (100 μg/mL) for 7 days and then switched to asymmetric conditions, i.e., with medium containing 20% FCS in the basal compartment and serum-free medium in the apical compartment.

Human umbilical vein endothelial cells (HUVECs) were obtained directly from umbilical cords donated by Bluets Maternity Hospital (Pierre Rouquès Hospital, Paris - Dr. Jessica Dahan Saal) or purchased from Lonza. These cells were cultured in flasks pre-coated with 10 μg/mL human fibronectin (Sigma-Aldrich) in endothelial basal medium (EBM-2) (Lonza), enriched with 2% fetal bovine serum (FBS) and endothelial cell growth supplement EGM-2 (BulletKit, Lonza). Before the addition of phage and/or treatments, confluent HUVECs were starved for 2 h in EBM-2 medium supplemented with 1% fetal calf serum without growth supplements (starvation medium) to stop cell proliferation. The cells were seeded in 24-well plates or on 12-well Transwell 3 μm-pore size filters (Sarstedt) and used up to passage 4.

Animal experimentation

All mice used in this study were C57BL/6J wild-type mice purchased from Charles River. Male mice aged 10–12 weeks were used for *ex vivo* experiments and 10-week-old female mice were used for *in vivo* studies. Animal experiments were conducted in accordance with institutional guidelines and approved by the local ethics committee and the French Ministry of Higher Education and Research (project n. Ce5/2020/004, authorization no. APAFIS#47879–2024030216059527). Mice were housed under specific pathogen-free (SPF) conditions at the Center de Recherche Saint-Antoine (Paris, France) and fed *ad libitum*.

Patients

Patients diagnosed with Crohn's disease and healthy subjects were enlisted from the Gastroenterology Department at Saint-Antoine Hospital in Paris, France. The study received approval from the competent ethics committee (Comité de Protection des Personnes Ile-de-France IV, IRB 00003835 Suivithèque study; registration number 2012/05NICB), and all subjects provided their consent after being fully informed. Our cohort consisted of 15 patients with Crohn's disease and 14 healthy controls. None of the subjects had received antibiotic treatment within the three months preceding sample collection or undergone intestinal surgery. The median age of the cohort was 38 ± 11 years. Further details of the cohort are presented in Table S3.

METHOD DETAILS

Phage preparation

Infections were initiated by adding phages to bacteria in the early exponential phase (OD_{600nm} = 0.2) at a multiplicity of infection (MOI) of 0.01. To enhance phage adsorption and amplification, LB media was supplemented with 1 mM $CaCl_2$ and $MgCl_2$. After overnight

incubation and lysis of the bacteria by the phages, remaining bacteria and debris were removed by centrifugation for 30 min at 3,000 × g, and the supernatant filtered sequentially through 0.45-μm and 0.2-μm cellulose acetate filters (VWR Avantor). Phages were concentrated by tangential flow filtration using a Vivaflow cassette system (Sartorius Stedim Biotech) and stored in a final solution of salt-magnesium (SM) buffer (17 mM $MgSO_4 \cdot 7H_2O$, 100 mM NaCl, 5 mM Tris-HCl (pH 7.5) at 4°C.

Lysates from the same bacteria cultured without phages were used as a mock negative control and were generated through a series of freeze/thaw cycles followed by sonication to closely mimic phage-induced lysis. The bacterial lysate was subsequently plated on LB agar plates to confirm the death of the bacteria. This sample then underwent the same processing steps used for phage purification.

Endotoxin removal and determination of the concentration

To effectively remove lipopolysaccharide (LPS), each preparation of purified phage or mock negative control were purified twice using Pierce high-capacity endotoxin removal resin (Thermo Fisher Scientific) and then three times using an EndoTrap HD kit (Lionex) according to the manufacturer's instructions. The final LPS concentration was determined using a Pierce Lyophilized Amebocyte Lysate (LAL) chromogenic endotoxin quantitation kit (Thermo Fisher Scientific) and was shown to be below 1 EU/mL when added to mammalian cells.

Experimental treatments to increase paracellular permeability in cell models

Caco-2/TC7 cells were treated with 5 mM EGTA (Sigma-Aldrich) in the apical compartment or human interferon-γ (IFNγ) and tumor necrosis factor-α (TNFα) (50 ng/mL each; Bio-Techne) in the basal compartment. The EGTA treatment was applied 2 h before adding the phages, whereas TNFα and IFNγ were applied 24 h before. HUVECs were treated with 10 ng/mL TNFα and IFNγ (Bio-Techne) added to the apical compartment of Transwell filters 18 h before phage addition.

Phage translocation assays in cell models

Phage translocation was evaluated by inoculating the apical side of the insert with between 10^7 and 10^9 plaques forming units (PFU) of purified phages at the beginning of the experiment. At each timepoint, 100 μL of medium from the basal side was collected to count the translocated phages by plaque assay. To count phages associated with the cells, Caco-2/TC7 or HUVECs were washed twice with phosphate buffered saline (PBS) to remove free phages and the cells were lysed by incubation in 1% Triton X-100 (Sigma-Aldrich) for 5 min and 100 μL of cell lysate was collected. Samples of basal medium and cell lysates were serially diluted in SM buffer, plated on LB agar plates overlaid with phage-specific *E. coli* strains (see above and Table 1), and the plates incubated at 37°C overnight to determine the number of PFU.

A mock negative control containing purified lysed bacteria without phages was also added to the cells to confirm that the observed effects were solely due to the presence of the phages (data not shown). In all experiments, the negative control consisted of cell culture medium only.

Permeability measurements

The paracellular permeability of Caco-2/TC7 and HUVECs monolayers was assessed by introducing 1 mg/mL 4 kDa FITC-dextran (FD4, TdB Consultancy) into the apical medium. Samples from the basal medium were collected at various timepoints, and the fluorescence measured at an excitation wavelength of 485 nm and an emission wavelength of 550 nm using a FLUOstar Omega microplate fluorometer (BMG Labtech), as previously described.[91] *Trans*-epithelial/*trans*-endothelial electrical resistance (TEER), which inversely correlates with ion permeability, was evaluated both before and after the addition of phages and/or treatment using a Volt-Ohm Meter (Millipore).

For HUVECs, permeability was also monitored in real time using the RTCA-DP xCELLigence system (Agilent), housed in a humidified incubator at 37°C with 5% CO2. The instrument measures electrical impedance on microelectrode-coated plates (Agilent) to track changes in barrier function. It was set to a single frequency of 10 kHz with 3-min measuring intervals over the course of 48 h.

Cytotoxicity assay and IL-8 secretion

At the end of the experiments, cytotoxicity was assessed by measuring lactate dehydrogenase activity in the apical medium, following the manufacturer's instructions (Cytotoxicity Detection KitPLUS, Roche). In addition, the level of the chemokine IL-8 in the basal medium of Caco-2/TC7 cells was quantified using an enzyme-linked immunosorbent assay (ELISA) kit *(R&D Systems).*

Preparation, purification and conjugation of CF488 fluorophore to M13 phages

M13 phage was produced by infecting *E. coli* TG1 grown to an OD_{600nm} = 0.4 with 10^{11} PFU of M13KO7 helper phages (New England BioLabs) for 2 h. After infection, 10 mL was transferred to a flask containing 400 mL LB supplemented with kanamycin (25 mg/L) and the flask was incubated for 24 h at 37°C with shaking. Phage purification was performed as previously described.[92] The bacterial culture was centrifuged at 12,000 × *g* for 30 min. The supernatant was supplemented with PEG 8000 (4% w/v) and NaCl (3% w/v) and incubated at 4°C for 90 min. The solution was then centrifuged for 15 min at 12,000 × *g* and the phage pellet was resuspended in PBS before a further purification step by isoelectric point (IEP) precipitation.[93] Purified phages were finally resuspended in PBS. Phage concentrations were determined by measurement of the absorbance at a wavelength of 269 nm in a UV-Vis spectrophotometer (extinction coefficient ε = 3.84 cm^2/mg) using a 320 nm wavelength spectrum as baseline.

An aliquot of 1 μmol CF 488A succinimidyl ester (CF488-SE; Biotium) was dissolved in 100 μL anhydrous DMSO to obtain a 10 mM CF488-SE solution. Then, 29.3 μL of the CF488-SE solution was added dropwise, with stirring, to 1 mL of 40 nM M13 phages in 100 mM sodium carbonate-bicarbonate buffer (pH 9). The reaction was carried out for 3 h at 25°C with shaking (ThermoMixer HC, S8012-0000; STARLAB, Hamburg, Germany). The CF488-tagged M13 phages were extensively dialyzed against 100 mM sodium carbonate-bicarbonate buffer (pH 9) using a regenerated cellulose membrane (14 kDa cut-off) to remove reaction by-products. The last dialysis cycle was performed against 10 mM PBS (pH 7.4).

Visualization of the endocytic pathway in HUVECs

To evaluate the endocytic process, transferrin-Cy3 (3.5 μg/mL; Cy3 ChromPure Human transferrin; Jackson ImmunoResearch Europe) was added to HUVECs simultaneously with the phages. Acidic compartments were visualized by staining the cells with Lysotracker Deep Red (200 nM; Thermo Fisher Scientific) either 30 min or 1 h prior to fixation.

Confocal microscopy

Caco-2/TC7 cells were fixed with 4% paraformaldehyde for 30 min and then permeabilized for 1 h with PBS containing 1% bovine serum albumin (BSA), and 0.5% Triton X-100 (Sigma-Aldrich), and finally blocked with PBS containing 3% BSA. HUVECs were fixed with 4% paraformaldehyde for 15 min, followed by permeabilization for 10 min in PBS containing 2% BSA and 0.1% Triton X-100 (Sigma-Aldrich), followed by blocking with 2% BSA. Cells were then incubated at 37°C with primary antibodies: tricellulin (1:200; MARVELD2 700191; Thermo Fisher Scientific), ZO-1 (1:200; ZO1-1A12; 33–9100 Thermo Fisher Scientific), and E-cadherin (1:500; ECCD2 M108; Takara Bio Europe). Alexa Fluor 647, and Alexa Fluor 546–conjugated anti–immunoglobulin G were used as secondary antibodies (1:400; Invitrogen, Thermo Fisher Scientific). Nuclei were stained with 4 -6-diamidino-2-phenylindole (DAPI) (1 μg/mL, Invitrogen), and actin with Alexa Fluor 647/546-labelled phalloidin (1:400; Invitrogen). Specimens were mounted in fluorescence mounting medium (ProLong, Gold Antifade, Thermo Fisher Scientific). Confocal laser scanning microscopy was carried out with an Olympus Fluoview FV3000 instrument using a ×60 oil immersion objective. To obtain Z stacks, optical sections were taken over 0.43 μm. Images were acquired by FV3000 software (Olympus) and processed using ImageJ Fiji (https://imagej.nih.gov/ij/). M13 phage-positive Caco-2/TC7 cells were analyzed using Qupath. Cells were segmented by setting a threshold of 10 to detect nuclei, followed by an expansion adjustment of 10 μm to define the cell boundaries. The Green Max signal was selected to identify M13 phage particles. Three fluorescence intensity thresholds were then applied to classify cells: 48 for low-positive (+), 100 for medium-positive (+), and 200 for high-positive (+). Cells were categorized based on these thresholds by analyzing 10 randomly selected images.

Ex vivo assays with Ussing chambers

Intestinal sections (terminal ileum and distal colon) were longitudinally excised and mounted in Ussing chambers (WorldPrecision Instruments, UK) as previously described.[94] Both the apical and basal chambers were filled with 2 mL Ringer buffer solution (115 mM NaCl, 25 mM $NaHCO_3$, 1.2 mM $MgCl_2$, 1.2 mM $CaCl_2$, 2.4 mM K_2HPO_4, 0.4 mM KH_2PO_4) and maintained at 37°C in a 95% oxygen/5% CO_2 atmosphere. Following a 20 min equilibration period, phages and FITC-Dextran 4 kDa (FD4) (final concentration: 2 mg/mL; TdB Consultancy) were introduced into the apical chamber. Intestinal permeability was assessed by measuring the fluorescence of FD4 in the basal compartment every 15 min, using a microplate fluorometer (BMG Labtech). Permeability values are expressed at each time point as the percentage of the amount of FD4 initially introduced into the apical chamber. To evaluate phage translocation, the apical chamber was inoculated with purified phages at the beginning of the experiment and phages from the basal compartment counted by plaque assay after 90 min, as detailed in the phage translocation assays in the ''cell models'' section.

DSS-induced colitis model in mice

Colitis was induced by administering 2% dextran sulfate sodium (DSS; MP Biomedicals) in drinking water for 7 days, followed by 2 days of recovery with regular water. Clinical colitis severity was assessed daily using the Disease Activity Index (DAI), which combines scores for body weight loss, stool consistency and the presence of blood in stools. The DAI ranges from 0 (no signs) to 12 (severe colitis). On day 9, mice received 200 μL of a phage cocktail via oral gavage, containing T4 phage (3.44×10^8 functional phages/mouse), M13yfp phage (5.5×10^8 functional phages/mouse) and ΦX174 phage (1.75×10^9 functional phages/mouse). Feces were collected, and mice were sacrificed at 1 h and 5 h post-gavage to match intestinal transit time in mice.[54–56,95] Tissues (small intestine, colon, liver and spleen) were collected to quantify phage presence by plaque assay.

Quantification of phages by qPCR

For qPCR, a 20 μL reaction mix was assembled with 50nM T4 phage primers (forward: 5 -ACTGGCCAGGTATTCGCA-3 , and reverse: 5 -ATGCTTCTTTAGCAGCGGCA-3) or M13 primers (forward: 5 - CACCGTTCATCTGTCCTCTTT -3 and reverse: 5 -CGACCTGCTCCATGTTACTTA-G -3) or ΦX174 primers (forward: 5 -GGTTCGTCAAGGACTGGTT-3 and reverse: 5 -TTGAACAG CATCGGACTCAG-3), SYBR Green PCR Master Mix (Applied Biossystems) and the sample. The qPCR reactions were run on a StepOnePlus Real-Time PCR System (Thermo Fisher Scientific) with the following cycling conditions: 95°C for 10 min, 40 cycles of 95°C for 15 s, and 60°C for 1 min, followed by a melt curve setting of one cycle of 95°C for 15 s, 60°C for 1 min and 95°C for

15 s. A calibration curve using T4 DNA (ranging from 3.1 to 1.10^{-8} ng) was used to determine the genome copy/mL of T4 phages in each sample. The conversion of qPCR results to copy number/mL followed the principles outlined by Peng et al.[96]

Sample collection

Blood was drawn into plasma collection tubes containing the anticoagulant EDTA (Dutscher) and promptly placed on ice, followed by centrifugation at 2,000 × g for 10 min to isolate the plasma, which was then filtered through a 0.45-μm cellulose acetate filter (VWR Avantor) and stored at −20°C. Stool samples were gathered directly into RNAlater (Sigma-Aldrich), which precipitates phage particles, and homogenized by vortexing with glass beads in a low-binding Eppendorf tube (Sigma-Aldrich). Following centrifugation at 20,000 × g for 15 min at 4°C, the supernatant was discarded, and the pellet was directly stored at −80°C. Both blood and stool samples from each subject were collected on the same day. For negative controls, sterile water was placed in a blood collection tube and in a low-binding tube.

Viral DNA isolation

Viral DNA isolation was carried out using a phenol/chloroform protocol adapted from Billaud et al.[97] Human stool samples (0.2 g) and plasma samples (3 mL) or murine samples. Human stool samples were resuspended in 7 mL 10 mM Tris pH 7.5. All samples were then centrifuged at 4,750 × *g* for 10 min at 4°C, and the supernatant was filtered through a 0.45-μm PES membrane filter to eliminate bacteria. The filtered supernatant was then treated with benzonase-nuclease (250 U) for 2 h at 37°C. Viruses were concentrated by mixing the samples with 0.5 M NaCl and 10% weight/volume PEG-8000, followed by overnight incubation at 4°C. Then, samples were centrifuged at 4,750 × g for 30 min at 4°C, and the resulting precipitate was collected and re-suspended in 400 μL 10 mM Tris pH 7.5. An equal volume of chloroform was added, and the samples were gently shaken to eliminate remaining bacteria and decrease extracellular vesicle contamination. Samples were centrifuged at 16,000 × g for 5 min at 4°C to extract the aqueous phase. To remove non-encapsidated nucleic acids, the samples were treated with 8 U TURBO DNAse I (Ambion/Thermo Fisher Scientific) and 20 U RNAse (Thermo Fisher Scientific). The DNAse was then inactivated with EDTA at a final concentration of 20 mM. To disrupt the capsids, 40 μg proteinase K and 20 μL 10% SDS were added before incubation at 56°C for 3 h. Subsequently, the samples were transferred into tubes containing an equal volume of phenol-chloroform-isoamyl alcohol (25:24:1, Thermo Fisher Scientific). After vigorous vortexing, they were centrifuged at 16,000 × g for 5 min at 4°C. The resulting aqueous phase was extracted and transferred to a new tube. Chloroform/isoamyl alcohol (24:1, Thermo Fisher Scientific) was added, followed by another identical centrifugation to eliminate traces of phenol. The resulting aqueous phase was then extracted, and the DNA was precipitated using 0.3 M sodium acetate, 2.5 volumes of ethanol, and glycogen (20 μg/mL final concentration), followed by a 1-h incubation at −20°C. Samples were then centrifuged at 16,000 × g for 30 min at 4°C, and the pellet was washed twice with 0.5 mL cold 75% ethanol. After ethanol removal, the dry pellet was resuspended in 10 mM Tris pH 8 and stored at −20°C.

DNA concentration was measured using a Qubit 4 Fluorometer (Invitrogen).

Viral DNA sequencing

Libraries were prepared using the xGen kit (Integrated DNA Technology), which includes a step to convert ssDNA to dsDNA with minimal bias.[98] The resulting libraries were then sequenced on an Illumina apparatus (paired-ended 150 bp reads), generating 9.2 million (±6 million) pairs of reads (Table S5).

Determination of vOTUs

Sequencing reads underwent cleaning using fastp 0.23.1[80] with the following parameters: –trim_front1 2 –trim_tail1 2 –trim_front2 15 –trim_tail2 2 -r -W 4 -M 20 -u 30 -e 20 -L 100. Human reads were eliminated by aligning the cleaned reads against the human genome (GRCh38) using bowtie2 2.4.1[77] with the –very-sensitive option. Four samples (H7_F, H10_F, H13_B, and CD7_B) were excluded from further analysis due to having less than 100,000 pairs of reads remaining.

Assembly was conducted using the cleaned, non-human reads both per subject (utilizing both blood and stool samples) and collectively from samples of all subjects. In both cases, paired-end and unpaired reads were used and deduplicated before assembly using the dedupe function of bbmap 38.86.[75] Assembly was performed using SPAdes 3.14.0[85] with default parameters, excluding contigs smaller than 2 kb, corresponding to the minimal size of DNA viral genomes.

Contigs were clustered to define operational taxonomic units (OTUs) using an approach adapted from Shah et al.[99] Initially, pairwise alignment of all contigs was performed using BLAT 36.[76] Contigs exhibiting a total alignment length against themselves >110% were identified as chimeras and removed. Then, clustering was performed at 95% average nucleotide identity (ANI), representing species boundaries, using scripts described in Shah et al.[99]

Two strategies were combined to detect viral OTUs: dedicated tools and sequence homology in virus databases. For the dedicated tools, VirSorter2 2.2.3[88] was used with specific parameters to enhance stringency: *–include-groups dsDNAphage, NCLDV,RNA,ssDNA, lavidaviridae –exclude-lt2gene –min-length 2000 –viral-gene-required –hallmark-required –min-score 0.9 –high-confidence-only*. VIBRANT 1.2.1[87] was also used. In addition, CheckV 0.8.1[79] was applied to all OTUs, with only those surpassing a "medium" viral quality being retained. For the databases, the OTUs were compared to sequences in various virus databases (GPD,[100] GVD,[101] COPSAC,[99] MGV,[102] CHVD,[103] and RefSeq Virus 07/2023[104]) using BLAT 36,[76] considering OTUs with

>90% ANI homology to at least one database as being viral. Finally, the OTUs from both methods were merged to create a non-redundant list of 17,454 viral OTUs (vOTUs). Complete information for each vOTU can be found in Lamy-Besnier et al.[32]

Characterization of the vOTUs

For classification, vOTUs were combined with the INPHARED database[105] (02/07/2023) before clustering with vContact2 0.9.19[86] using default parameters. A classification was assigned from the obtained network using graphanalyzer 1.5.1.[81]

Host prediction was conducted using iPHoP 1.2.0[82] with the associated database (09/2021) using default parameters.

Ecological analysis

Cleaned, non-human reads underwent mapping using bwa-mem2 2.2.1[78] against all OTUs with default parameters. The resulting SAM file was converted to BAM and sorted by read name using samtools[84] 1.9 before filtering out low-quality alignments using msamtools filter 1.1.3. Alignments were retained if they were >80 bp long, had >95% overall identity, and >80% of the read aligned. Only the best alignment (or alignments in cases of ties) for each read was retained.

Alignments were then converted into counts using msamtools profile, with the multi = proportional option to distribute reads mapping to different OTUs according to their relative abundance. The coverage and depth of each OTU for each sample were determined using msamtools coverage. OTUs with coverage <50% of the OTU size or an average depth <1 in a given sample were removed.

For viral community analysis, vOTU counts were extracted. vOTUs present in negative control samples were removed from the other samples. Counts were then normalized by vOTU length and transformed into relative abundance for comparison across vOTUs and samples, forming the primary abundance table for analysis. This relative abundance table was analyzed using the R package phyloseq[83] 1.46.0.

QUANTIFICATION AND STATISTICAL ANALYSIS

Statistical analyses were performed using GraphPad Prism (GraphPad Software). The assumption of normality was assessed using the Shapiro–Wilk test. Two group comparisons were performed using Student's *t* test (parametric) or Mann-Whitney test (nonparametric) and comparisons involving multiple groups were carried out using one-way analysis of variance (ANOVA) or Kruskal–Wallis test when the assumptions of ANOVA were not met. Spearman's test was used to assess the correlation between the two variables tested. A level of $p < 0.05$ was considered significant.

Cell Reports, Volume *45*

Supplemental information

Differential translocation of bacteriophages across the intestinal barrier in health and Crohn's disease

Clara Douadi, Quentin Lamy-Besnier, Ilias Theodorou, Olivier Schiettekatte, Yanis Sbardella, Loïc Brot, Paolo Emidio Costantini, Roberto Saporetti, Alberto Danielli, Matteo Calvaresi, Marianne De Paepe, Harry Sokol, Diego Garcia-Weber, Véronique Carrière, Sophie Thenet, and Luisa De Sordi

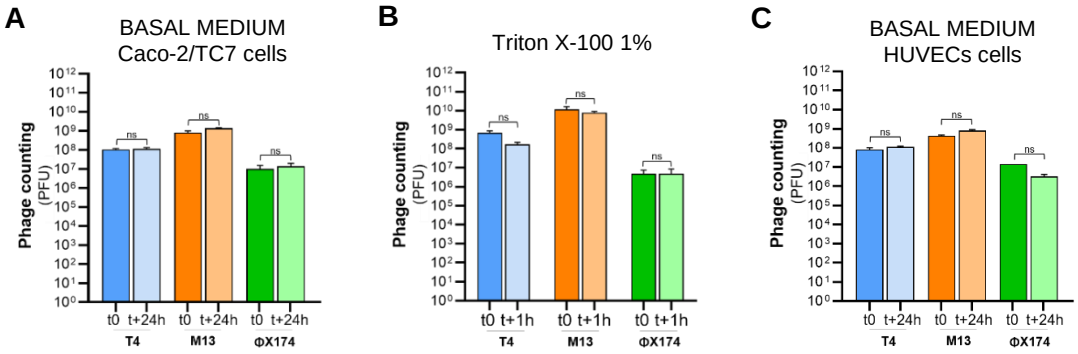

Figure S1 : Cell culture medium and Triton X-100 do not impact phage viability

(A) Titration of T4, M13, and ΦX174 phages immediately after suspension (t0) and 24 h after incubation in Caco-2/TC7 culture medium. **(B)** Titration of T4, M13, and ΦX174 phages immediately after suspension (t0) and following a 1 h incubation with 1% Triton X-100 (t+1h), used in this study to lyse eukaryotic cells. **(C)** Titration of T4, M13, and ΦX174 phages immediately after suspension (t0) and 24 h after incubation in HUVEC culture medium (t+24h). All experiments were performed in triplicates [n = 3]. Data are represented as mean ± SEM.

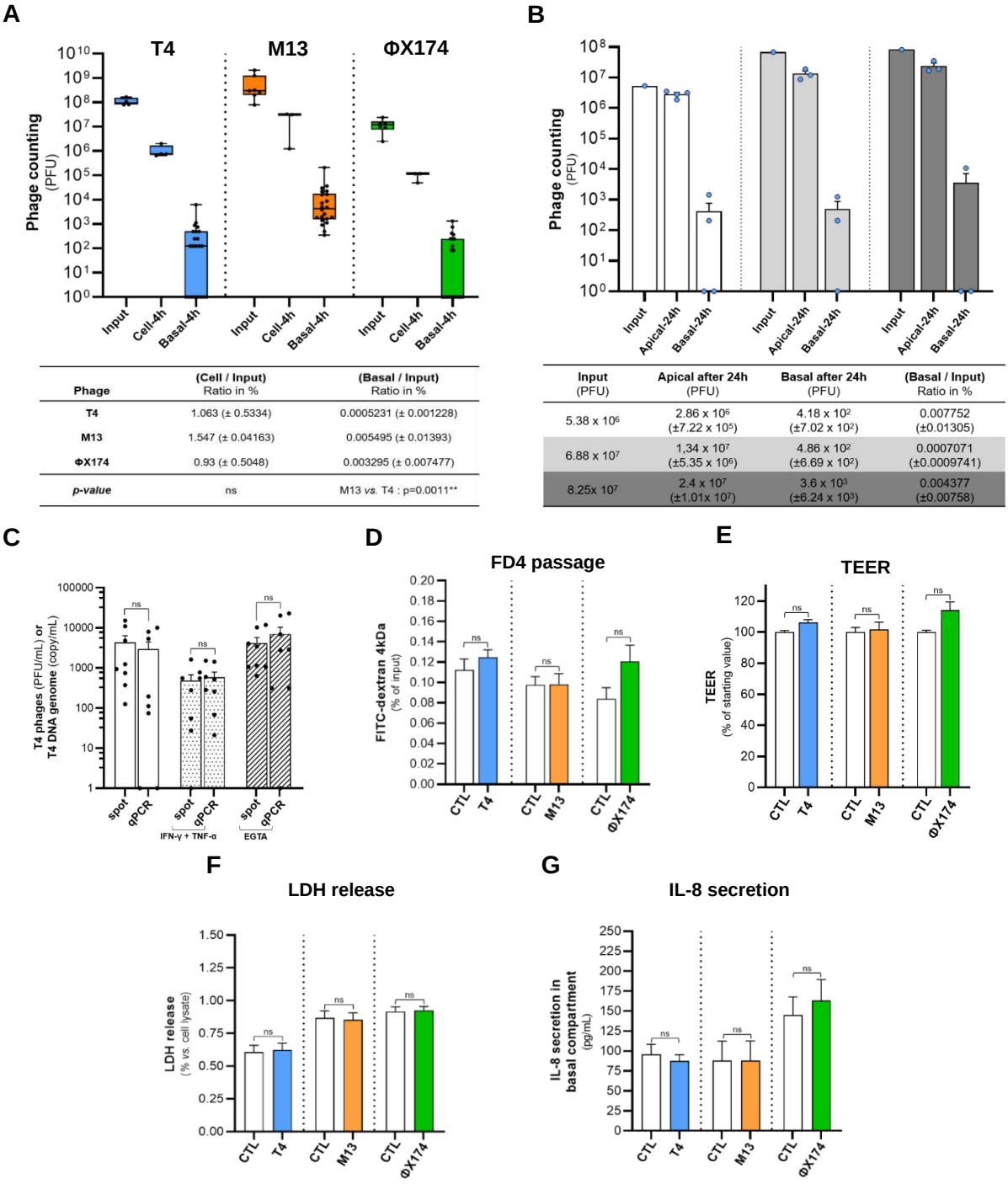

Phage	(Cell / Input) Ratio in %	(Basal / Input) Ratio in %
T4	1.063 (± 0.5334)	0.0005231 (± 0.001228)
M13	1.547 (± 0.04163)	0.005495 (± 0.01393)
ΦX174	0.93 (± 0.5048)	0.003295 (± 0.007477)
p-value	ns	M13 *vs.* T4 : p=0.0011**

Input (PFU)	Apical after 24h (PFU)	Basal after 24h (PFU)	(Basal / Input) Ratio in %
5.38×10^6	2.86×10^6 ($\pm 7.22 \times 10^5$)	4.18×10^2 ($\pm 7.02 \times 10^2$)	0.007752 (±0.01305)
6.88×10^7	$1{,}34 \times 10^7$ ($\pm 5.35 \times 10^6$)	4.86×10^2 ($\pm 6.69 \times 10^2$)	0.0007071 (±0.0009741)
8.25×10^7	2.4×10^7 ($\pm 1.01 \times 10^7$)	3.6×10^3 ($\pm 6.24 \times 10^3$)	0.004377 (±0.00758)

Figure S2 : Internalization, translocation and functionality of phages crossing Caco-2/TC7 intestinal epithelial cells and absence of impact on permeability, cytotoxicity, or inflammation (legend on following page)

Figure S2 : Internalization, translocation and functionality of phages crossing Caco-2/TC7 intestinal epithelial cells and absence of impact on permeability, cytotoxicity, or inflammation

(A) Titration of T4, M13, and ΦX174 phages associated to Caco-2/TC7 cells (cell) and translocated phages (basal) after 4 h of incubation in the apical compartment. The input refers to the phages initially added to the apical compartment. The table displays the percentage of phages associated to and translocated across Caco-2/TC7, calculated relative to the input. A minimum of four independent experiments [n ≥ 4] were performed. **(B)** Titration of T4 phages in the apical and basal compartments after 24 h of incubation following their addition to the apical compartment. The input refers to the number of phages initially added to the apical compartment. The table shows the initial input of T4 phages, the number of phages recovered from both the apical and basal compartments after 24 h, and the percentage of phages translocating across the Caco-2/TC7 monolayer, calculated relative to the input. One independent experiment was conducted in triplicate or quadruplicate. **(C)** Titration of T4 phages in the basal compartment after 24 h of apical incubation, measured by plaque assays (spot) and qPCR (a calibration curve using T4 DNA was used to determine the genome copy/mL) under both physiological, or compromised barrier conditions (IFN-γ + TNF-α, and EGTA). Two independent experiments were conducted in quadruplicate. **(D)** FITC-Dextran 4 kDa (FD4) passage from the apical to the basal compartment during 24 h in the presence of the indicated phage compared to control (CTL) condition without phage. **(E)** Measure of transepithelial electrical resistance (TEER) after 24 h of incubation with medium containing no phages (CTL) or the indicated phages. Values are expressed as a percentage relative to the starting value for each well and then normalized to the control condition. **(F)** Release of lactate dehydrogenase (LDH) by the cells in the apical compartment, after 24 h of incubation with medium containing no phages (CTL) or the indicated phages. Values are expressed as the percentage of LDH measured in the whole cell lysate. **(G)** Secretion of pro-inflammatory cytokine IL-8 by the cells within the basal compartment after 24 h of incubation with medium containing no phages (CTL) or the indicated phages. For all the experiments, a minimum of four independent experiments [n ≥ 4] were performed. All data are represented as mean ± SEM.

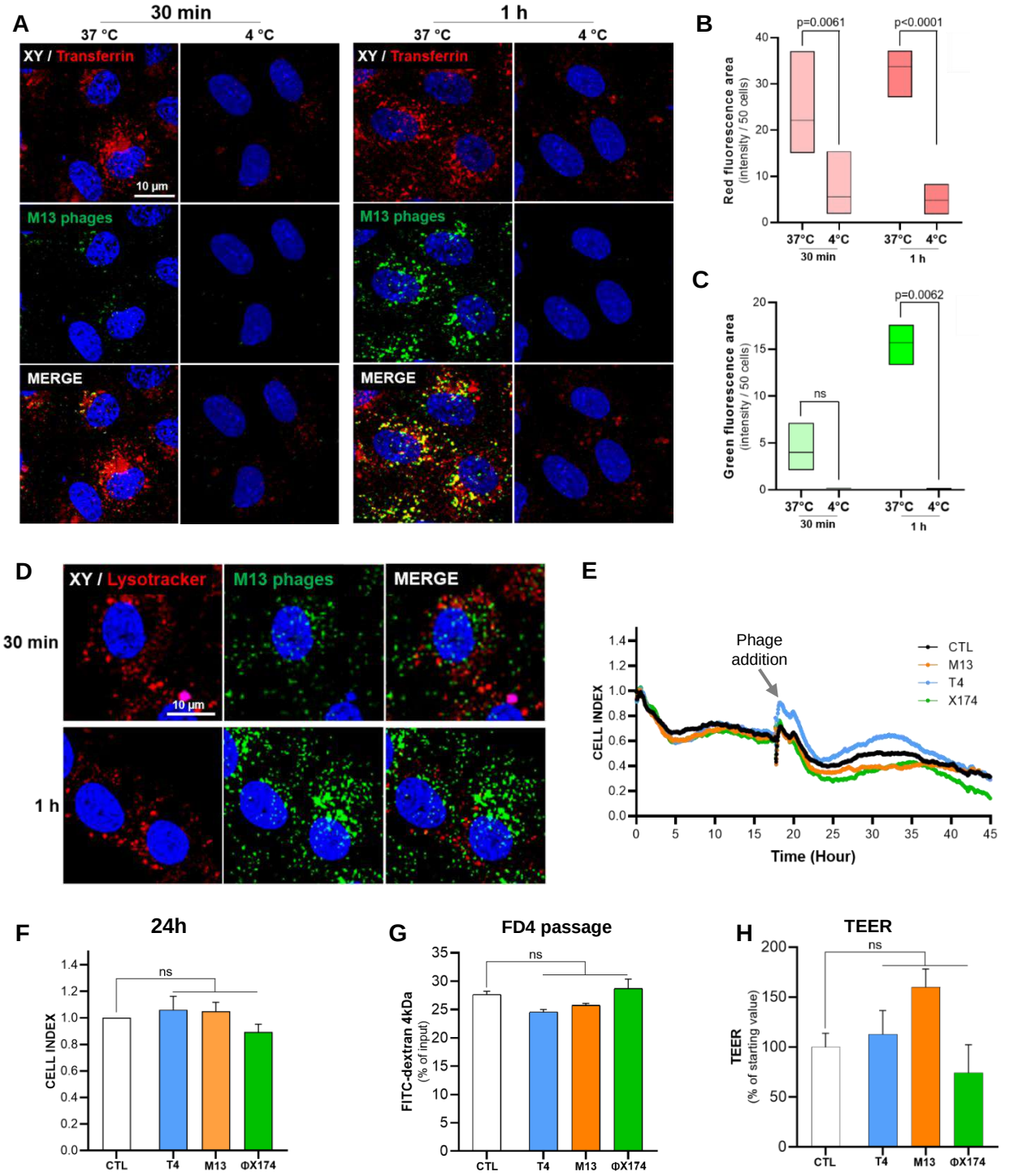

Figure S3 : Visualization of phages in the endocytic pathway in HUVECs cells following short incubation periods and phage impact on cellular permeability

(A) Images of CF488-labeled M13 phages and Cy3-labeled transferrin in HUVECs after 30 min and 1 h, at 37°C, and 4°C. Quantification of the **(B)** red fluorescence area (transferrin), and **(C)** green fluorescence area (M13 phages) in HUVECs following 30 min and 1 h, at 37°C, and 4°C, as shown in panel (A). Data represent mean values obtained from analysis of 5 randomly selected images. **(D)** Images of CF488-labeled M13 phages and Lysotracker Deep Red in HUVECs after 30 min and 1 h. For A and D: scale bar, 10 µm. **(E)** Representative plot of real-time permeability (cell index) of HUVECs in presence of the indicated phage relative to control (CTL) condition using xCELLigence system. **(F)** Cell index values obtained after 24 h in presence of the indicated phage relative to control (CTL) condition without phage after real time measure of HUVECs permeability, shown in panel (E). **(G)** FITC-Dextran 4 kDa (FD4) passage from the apical to the basal compartment after 24 h in presence of the indicated phage relative to control (CTL) condition. **(H)** Measure of transendothelial electrical resistance (TEER) after 24 h of incubation with medium containing no phages (CTL) or the indicated phages. Values are expressed as the percentage relative to the starting value for each well and then normalized to the control condition. For (E) to (H), three independent experiments [n=3] were performed. Data are represented as mean ± SEM.

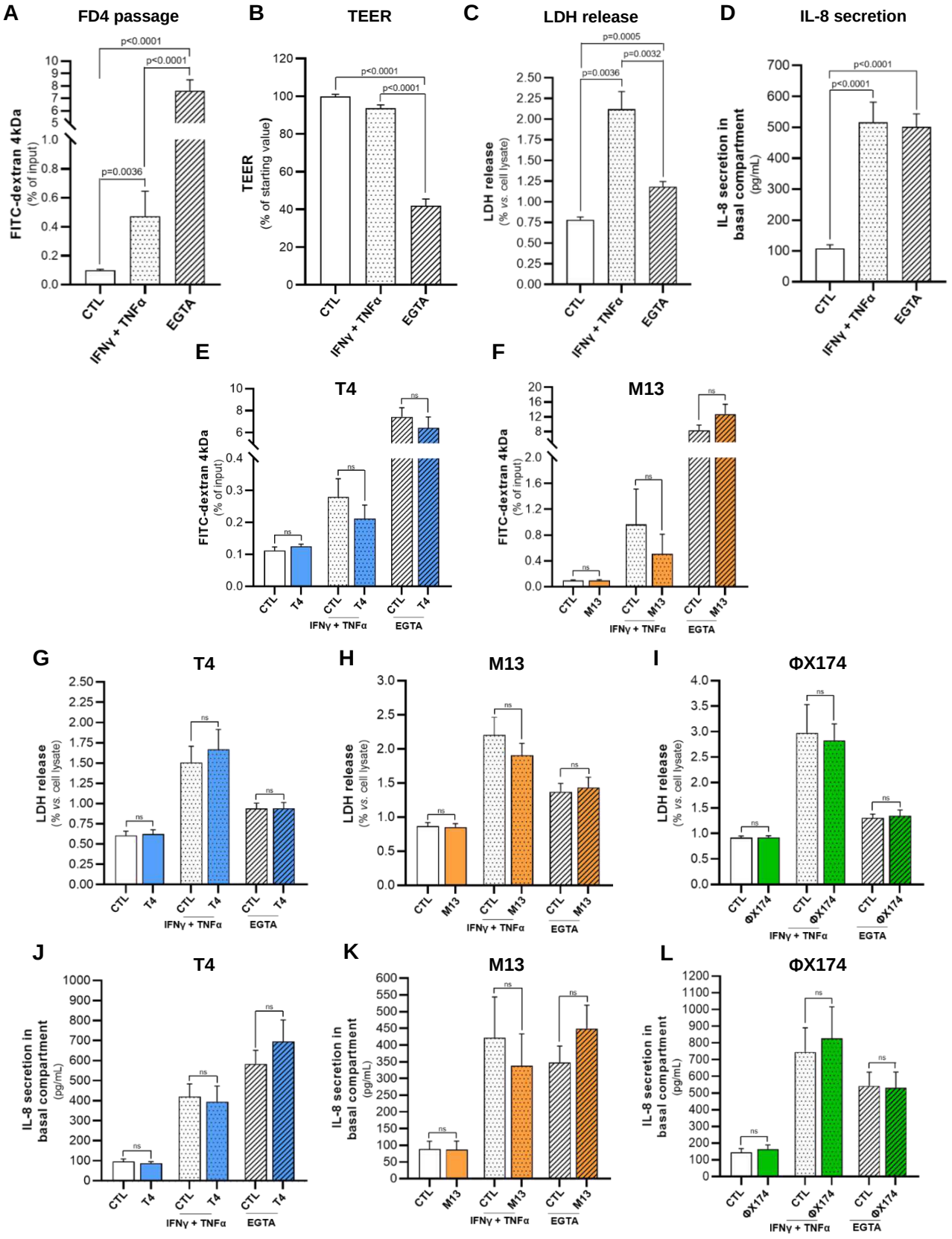

Figure S4 : Phages do not induce hyperpermeability, cytotoxicity, or inflammation in Caco-2/TC7 cells under compromised barrier conditions (legend on following page)

Figure S4 : Phages do not induce hyperpermeability, cytotoxicity, or inflammation in Caco-2/TC7 cells under compromised barrier conditions

Caco-2/TC7 were treated with IFNγ + TNFα in the basal compartment during 48 h, or with EGTA in the apical compartment during 26 h. **(A)** FITC-Dextran 4 kDa (FD4) passage from the apical to the basal compartment (24 h of FD4 flux). **(B)** Measure of transepithelial electrical resistance (TEER). Values are expressed as a percentage relative to the starting value for each well and then normalized to the control condition. **(C)** Release of lactate dehydrogenase (LDH) from cells (expressed as the percentage of LDH measured in the whole cell lysate). **(D)** Secretion of pro-inflammatory cytokine IL-8 by the cells into the basal compartment. For (A) to (D), these data were pooled from control groups used in independent experiments involving T4, M13, and ΦX174 phages, with at least 3 independent experiments conducted for each [n ≥ 9]. Data are represented as mean ± SEM. **(E-F)** FITC-Dextran 4 kDa (FD4) passage from the apical to the basal compartment during 24 h in presence of **(E)** T4, or **(F)** M13 phages relative to control (CTL) condition, under healthy, and compromised barrier conditions (IFNγ + TNFα, or EGTA). (**G-I**) Release of lactate dehydrogenase (LDH) from cells after 24 h in presence of **(G)** T4, **(H)** M13, or **(I)** ΦX174 phages relative to control (CTL) condition, under healthy, and compromised barrier conditions (IFNγ + TNFα, or EGTA). (**J-L**) Secretion of pro-inflammatory cytokine IL-8 by the cells into the basal compartment after 24 h in presence of **(J)** T4, **(K)** M13, or **(L)** ΦX174 phages relative to control (CTL) condition, under healthy, and compromised barrier conditions (IFNγ + TNFα, or EGTA). For (E) to (L), a minimum of three independent experiments [n ≥ 3] were performed. Data are represented as mean ± SEM.

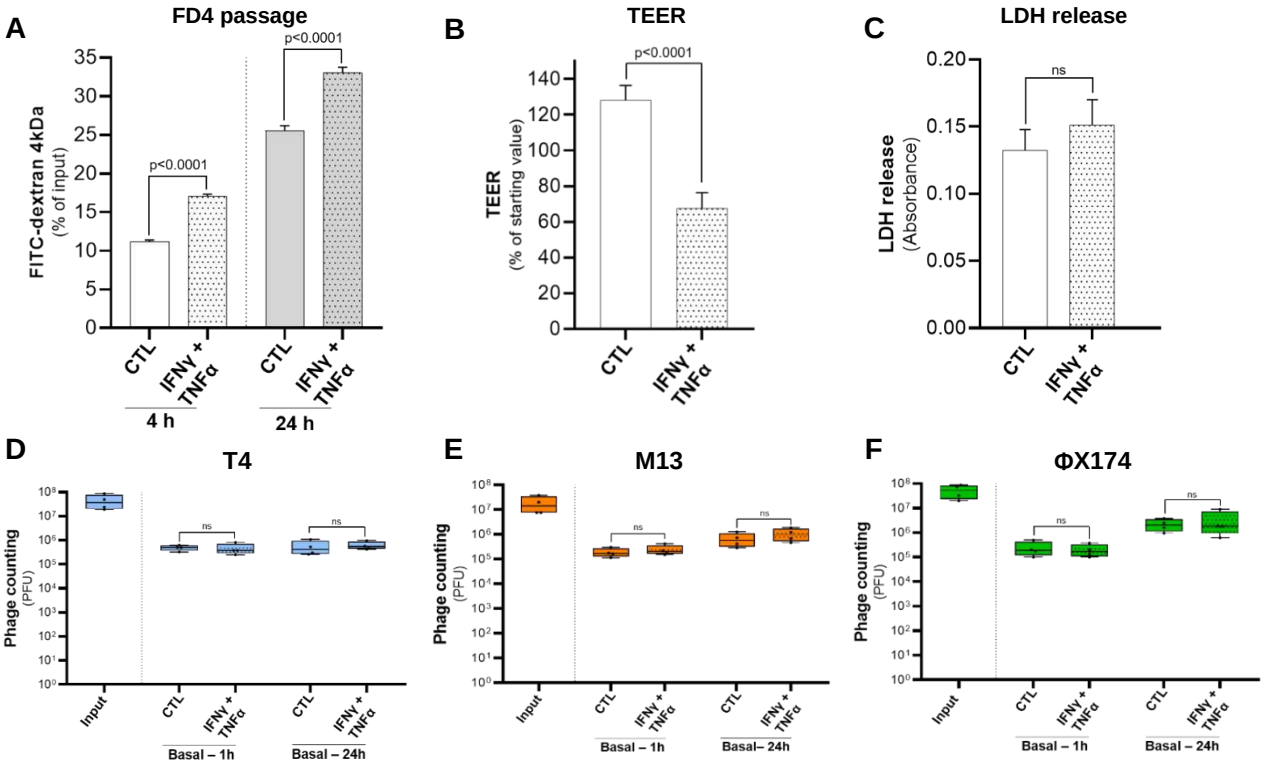

Figure S5 : Phage translocation is not impacted by inflammatory condition in HUVECs cells
(A) FITC-Dextran 4 kDa (FD4) passage from the apical to the basal compartment after 22 h (4 h of FD4 flux), and 42 h (4 h of FD4 flux) of IFNγ + TNFα treatment. **(B)** Measure of transendothelial electrical resistance (TEER) after 18 h of IFNγ + TNFα treatment. Values are expressed as a percentage relative to the starting value for each well and then normalized to the control condition. **(C)** Release of lactate dehydrogenase (LDH) from cells after 42 h of IFNγ + TNFα treatment. For (A), (B), (C), experiments were pooled from control groups used in independent experiments involving T4, M13, and ΦX174 phages [n = 9]. **(D-F)** Titration of **(D)** T4, **(E)** M13, and **(F)** ΦX174 phages in the basal compartment (basal) after 24 h of incubation. The input represents the phages added in the apical compartment at the beginning of the experiment. Conditions include healthy barrier condition (CTL) relative to compromised barriers conditions induced by IFNγ and TNFα. For (D), (E), (F), three independent experiments [n = 3] were performed. Data are represented as mean ± SEM.

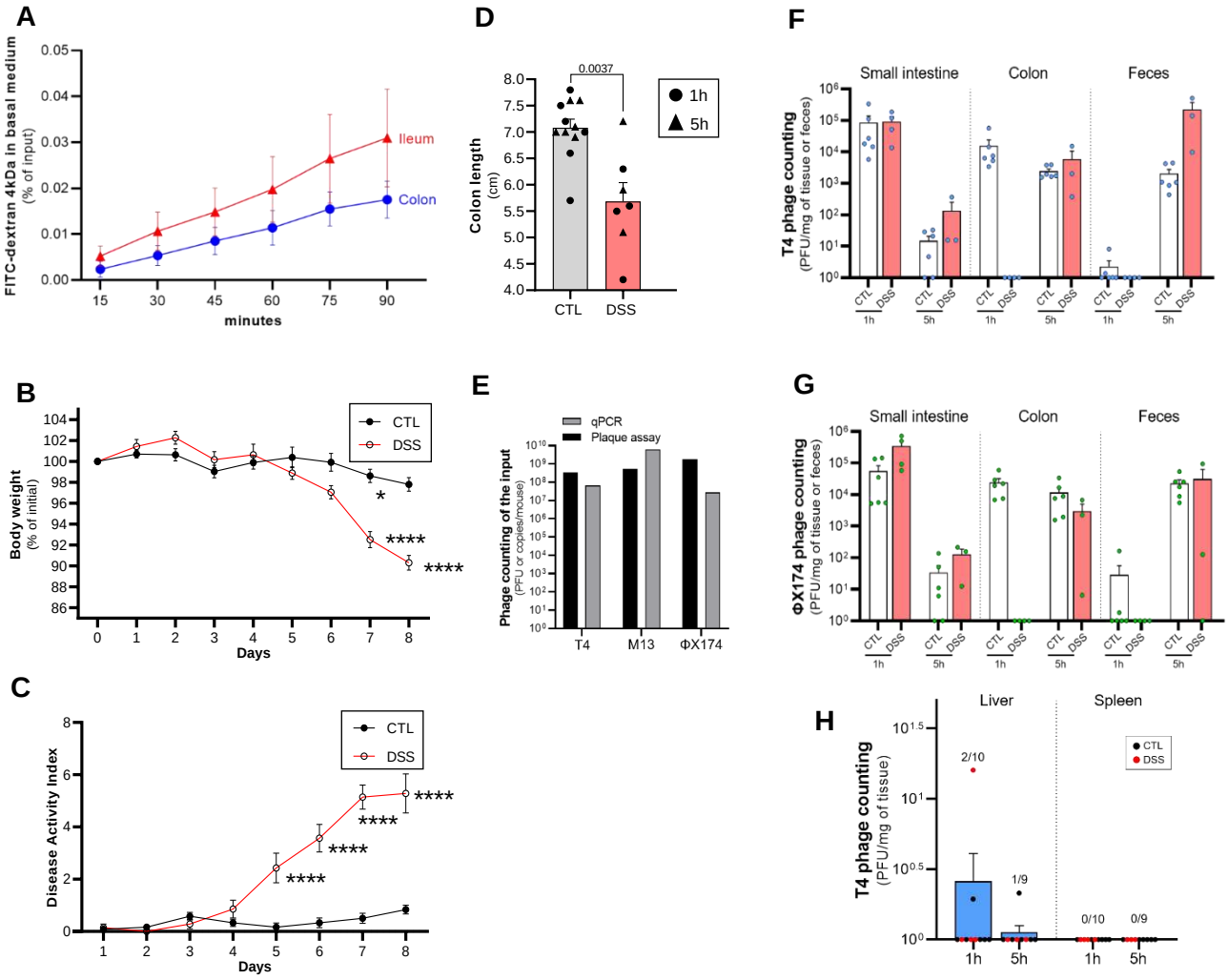

Figure S6 : Phage translocation in mice models

(A) Level of FITC-Dextran 4kDa (FD4) in basal medium over 90 min for ileum (red curve) and colon (blue curve) tissues from healthy mice in the *ex vivo* Ussing chamber model. For each intestinal segment, six replicates were performed. Data are represented as the percentage of fluorescent tracer added in the apical chamber over time and as mean ± SEM. **(B)** Bodyweight changes in control and DSS-treated mice throughout the *in vivo* experiment. **(C)** Disease Activity Index (DAI) scores in control and DSS-treated mice. **(D)** Colon length measured at day 9 in both groups. Symbols indicate the mice sacrified either 1 h (circles) or 5 h (triangles) after phage cocktail oral gavage. **(E)** Titration of T4, M13 and ΦX174 phages in the input sample by plaque assays and qPCR. **(F-G)** Titration of T4 **(F)** or ΦX174 **(G)** phages in the small intestine, colon and feces of control and DSS-treated mice at 1h and 5 h post-oral administration. **(H)** Titration of T4 phages in the liver and spleen of control and DSS-treated mice, 1h and 5 h after oral administration. Numbers indicate mice positive for phage detection out of the total tested. Phage quantification in (F), (G) and (H) was performed by plaque assays. Data are represented as mean ± SEM ; n = 6 mice per control group (1h and 5h post-gavage) and n = 3 or 4 mice per DSS-treated group (1h and 5h post-gavage).

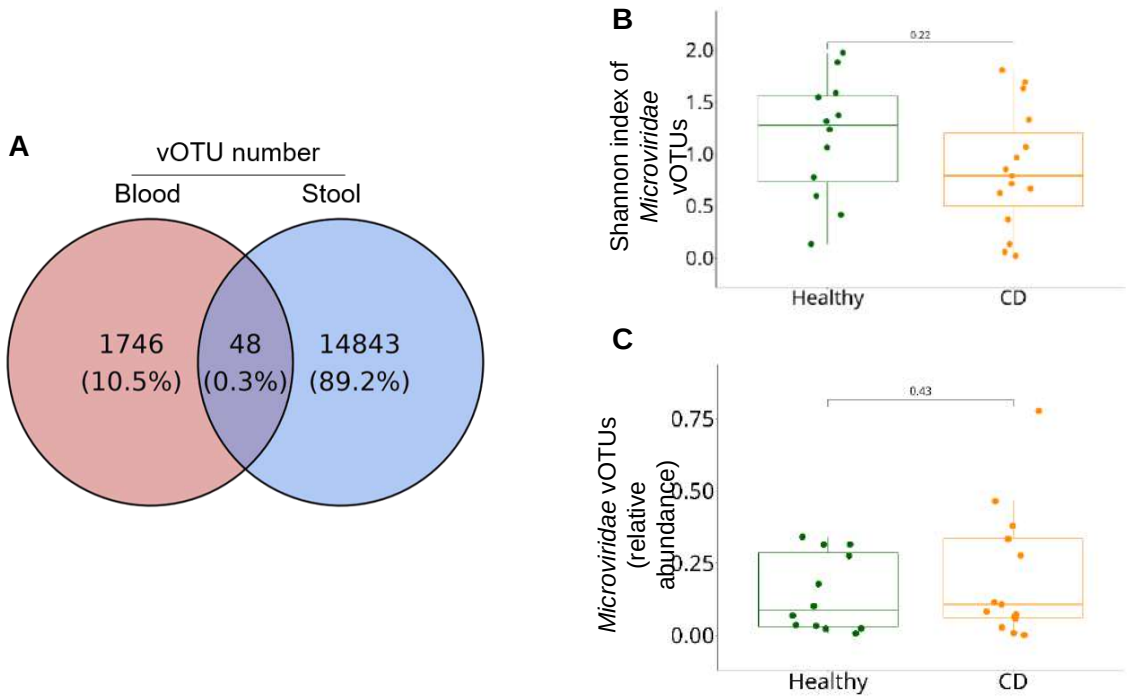

Figure S7 : vOTUs identified in blood and fecal samples from all participants and analysis of fecal *Microviridae.*
(A) Venn diagram of the vOTUs identified in blood and fecal samples from all participants. The final vOTU dataset was obtained by excluding all sequences detected in the negative controls and retaining only those present in at least one biological sample across the 29 participants in the cohort. **(B)** Alpha diversity of *Microviridae* in fecal samples, quantified using Shannon index, and compared between patients with Crohn's disease (CD) and healthy subjects. (**C)** Overall relative abundance of *Microviridae* vOTUs in fecal samples, separated by disease status.

Table S1 : Phages do not induce hyperpermeability of Caco-2/TC7 cells in compromised barrier conditions. Measure of transepithelial electrical resistance (TEER) after 24 h of incubation with medium containing no phages (CTL), or the indicated phages, under healthy, and compromised barrier conditions (IFNγ + TNFα or EGTA treatment). A minimum of three independent experiments [n ≥ 3] were performed. Values are expressed as a percentage relative to the starting value for each well, and then compared to the control condition.

TEER (% of starting value)						
	CTL	**T4**	**CTL**	**M13**	**CTL**	**ΦX174**
	100 (± 3.643)	106.2 (± 6.758)	100 (± 9.452)	101.7 (± 14.86)	100 (± 3.649)	114.3 (± 14.49)
p-value	p>0.99		p>0.99		p>0.99	
IFNγ + TNFα	97.27 (± 7.581)	105.8 (± 16.78)	90.77 (± 10.82)	89.99 (± 7.991)	91.35 (± 10.91)	92.82 (± 7.656)
p-value	p>0.99		p>0.99		p>0.99	
EGTA	48.04 (± 13.02)	58.29 (± 20.81)	31.06 (± 16.16)	22.72 (± 11.42)	45.9 (± 28.30)	46.80 (± 30.25)
p-value	p>0.99		p>0.99		p>0.99	

Table S2 : Percentage of translocated phages across intestinal tissue in healthy mice.
Percentage of phages that translocated after 90 min of addition in the apical compartment using the Ussing chamber system, calculated relative to the input. For each phage, three ileum and colon tissue samples taken from two or three individual mice were analyzed.

Phage	**Ileum (Basal / Input)** Ratio in %	**Colon (Basal / Input)** Ratio in %
T4	0.0008730 (± 0.001496)	0.0004333 (± 0.0005859)
M13	9.348e-005 (± 0.0001615)	1.207e-005 (± 0.00001987)
ΦX174	0.0004167 (± 0.0007217)	0
p-value	ns	ns

Table S3 : Detailed information about the participants included in the study.
"CD" indicates patient with Crohn's disease and "H" indicates healthy subject

Participant	Sampling date	Sex	Age	Age at diagnosis	Localisation (Montreal)	Flare/ Remission	C-reactive protein (mg/L)	Harvey-Bradshaw Index	Smoking	Surgery	Antibiotic (last month)	Undergoing treatment
CD1	2020	Female	53	37	L2	Remission	1	2	Past	No	No	Yes
CD2	2020	Female	40	NA	E3	Remission	1	NA	Past	No	No	No
CD3	2020	Female	38	NA	L3L4	Flare	1	4	Never	No	No	No
CD4	2020	Male	44	NA	L3L4	Remission	0.6	1	Never	No	No	No
CD5	2020	Female	40	20	L3	Remission	5	2	Past	No	No	Yes
CD6	2020	Male	60	55	L3	Flare	5	7	Never	No	No	Yes
CD7	2019	Female	26	16	L3	Flare	89.9	NA	Past	No	No	No
CD8	2020	Male	42	13	L3	Flare	6.3	3	Never	No	No	Yes
CD9	2020	Male	47	12	L2	Remission	7.8	0	Past	No	No	No
CD10	2018	Female	50	47	L1	Remission	1	NA	Current	No	No	Yes
CD11	2020	Female	33	19	L3	Flare	5.3	NA	Past	No	No	No
CD12	2020	Male	22	20	L3	Remission	5	3	Never	No	No	Yes
CD13	2020	Male	56	52	L1	Flare	8.7	7	Past	No	No	Yes
CD14	2020	Female	56	20	L3	Remission	1	2	Never	No	No	Yes
CD15	2020	Female	37	27	L3	Flare	1	7	Past	No	No	No
H1	2020	Female	26	NA	NA	NA	NA	NA	Never	No	No	No
H2	2020	Female	28	NA	NA	NA	NA	NA	Never	No	No	No
H3	2020	Male	31	NA	NA	NA	NA	NA	Never	No	No	No
H4	2020	Male	29	NA	NA	NA	NA	NA	Never	No	No	No
H5	2020	Male	36	NA	NA	NA	NA	NA	Never	No	No	No
H6	2021	Female	25	NA	NA	NA	NA	NA	Current	No	No	No
H7	2021	Male	32	NA	NA	NA	NA	NA	Never	No	No	No
H8	2021	Female	38	NA	NA	NA	NA	NA	Current	No	No	No
H9	2021	Female	27	NA	NA	NA	NA	NA	Never	No	No	No
H10	2021	Female	29	NA	NA	NA	NA	NA	Never	No	No	No
H11	2021	Female	56	NA	NA	NA	NA	NA	Never	No	No	No
H12	2021	Female	41	NA	NA	NA	NA	NA	Never	No	No	No
H13	2021	Female	28	NA	NA	NA	NA	NA	Never	No	No	No
H14	2021	Female	55	NA	NA	NA	NA	NA	Never	No	No	No

Table S4. Characteristics of the 16 vOTUs detected both in fecal and blood samples retrieved from the same subject (shared blood/fecal vOTUs).

"CD" indicates patient with Crohn's disease and "HS" indicates healthy subject.

"NA" indicates values that could not be assigned. Phages encoding an integrase in their genome were classified as temperate, while those lacking an integrase were considered virulent, excepted for *Microviridae* that were excluded from this analysis.

Name of the vOTUs	Family	Lifestyle	Host Phylum	Homology with known gut viruses	Participant
SampleCD8_ Contig922	NA	Virulent	Bacillota	Yes	CD
SampleH14_ Contig702	NA	Temperate	Bacteroidota	Yes	CD
SampleCD11_ Contig2059	*Anelloviridae*	Virulent	NA	Yes	CD
SampleCD11_ Contig727	*Microviridae*	NA	NA	Yes	CD
CrossAssembly_ Contig15411	*Microviridae*	NA	Bacillota	Yes	CD
SampleH2_ Contig566	NA	Virulent	Bacteroidota	Yes	CD
SampleH14_ Contig1913	NA	Temperate	Bacillota	Yes	HS
SampleH1_ Contig1177	NA	Virulent	NA	Yes	HS
SampleH13_ Contig1617	NA	Virulent	Bacillota	No	HS
SampleCD2_ Contig30	*Suoliviridae*	Virulent	NA	Yes	CD
SampleCD2_ Contig5485	NA	Virulent	NA	Yes	CD
CrossAssembly_ Contig3237	*Autographiviridae*	Virulent	Pseudomonadota	Yes	CD
CrossAssembly_ Contig8120	*Autographiviridae*	Virulent	Pseudomonadota	Yes	CD
SampleH1_ Contig422	*Microviridae*	NA	Bacteroidota	Yes	CD
CrossAssembly_ Contig1712	Unclassified	Temperate	Bacillota	No	CD
SampleCD10_ Contig6328	NA	Virulent	Bacillota	No	CD

Table S5 : Number of pairs of reads per sample.

The number of pairs obtained after sequencing is indicated in the "Raw" column. The number of pairs remaining after quality-filtering, and removal of non-human reads is indicated in the "Clean and non-human" column. The samples with less than 100,000 pairs of clean, and non-human reads were excluded from the analysis. “CD” indicates patient with Crohn’s disease and “H” indicates healthy subject

SampleName	Status	Sample Type	Raw	Clean and non-human
H1_F	Healthy	Stool	4 557 777	3 302 598
H2_F	Healthy	Stool	5 141 556	3 538 237
H3_F	Healthy	Stool	4 575 463	3 314 041
H4_F	Healthy	Stool	5 006 463	3 702 841
H5_F	Healthy	Stool	6 630 408	4 868 696
H6_F	Healthy	Stool	6 043 597	4 533 278
H7_F	Healthy	Stool	149	113
H8_F	Healthy	Stool	12 607 586	10 702 899
H9_F	Healthy	Stool	4 957 375	4 008 417
H10_F	Healthy	Stool	161	122
H11_F	Healthy	Stool	47 423 047	36 124 946
H12_F	Healthy	Stool	3 848 503	3 021 191
H13_F	Healthy	Stool	3 944 094	3 101 396
H14_F	Healthy	Stool	10 220 371	8 099 646
CD1_F	Crohn	Stool	3 398 455	2 610 231
CD2_F	Crohn	Stool	11 438 302	8 205 616
CD3_F	Crohn	Stool	27 092 512	19 524 928
CD4_F	Crohn	Stool	18 270 751	12 128 024
CD5_F	Crohn	Stool	8 453 588	5 729 131
CD6_F	Crohn	Stool	4 522 582	3 789 808
CD7_F	Crohn	Stool	2 985 683	2 478 116
CD8_F	Crohn	Stool	10 219 909	8 279 831
CD9_F	Crohn	Stool	7 091 001	5 360 552
CD10_F	Crohn	Stool	9 143 203	7 378 428
CD11_F	Crohn	Stool	9 290 609	7 084 801
CD12_F	Crohn	Stool	6 350 692	5 222 735
CD13_F	Crohn	Stool	7 983 876	6 487 386
CD14_F	Crohn	Stool	636 447	498 993
CD15_F	Crohn	Stool	3 500 715	2 724 997
H1_B	Healthy	Blood	25 145 743	6 790 645
H2_B	Healthy	Blood	13 872 445	5 336 467
H3_B	Healthy	Blood	17 469 863	6 122 420
H4_B	Healthy	Blood	16 038 090	3 433 116
H5_B	Healthy	Blood	19 342 807	5 840 315
H6_B	Healthy	Blood	1 916 528	185 563
H7_B	Healthy	Blood	2 347 924	837 299
H8_B	Healthy	Blood	2 733 222	788 996
H9_B	Healthy	Blood	2 689 347	723 438
H10_B	Healthy	Blood	2 486 126	573 092
H11_B	Healthy	Blood	1 397 921	160 240
H12_B	Healthy	Blood	3 711 044	691 480
H13_B	Healthy	Blood	2 312 559	68 548
H14_B	Healthy	Blood	5 506 340	2 713 132
CD1_B	Crohn	Blood	25 941 062	8 696 199
CD2_B	Crohn	Blood	14 183 825	8 720 837
CD3_B	Crohn	Blood	29 669 303	14 833 794
CD4_B	Crohn	Blood	20 129 214	11 955 938
CD5_B	Crohn	Blood	16 967 073	10 236 927
CD6_B	Crohn	Blood	4 631 975	1 917 021
CD7_B	Crohn	Blood	2 048 220	12 333
CD8_B	Crohn	Blood	7 197 457	3 434 820
CD9_B	Crohn	Blood	6 813 381	3 293 988
CD10_B	Crohn	Blood	6 542 891	3 338 429
CD11_B	Crohn	Blood	7 374 010	2 778 364
CD12_B	Crohn	Blood	9 614 014	4 117 958
CD13_B	Crohn	Blood	5 606 138	2 207 758
CD14_B	Crohn	Blood	5 555 652	2 052 908
CD15_B	Crohn	Blood	8 436 207	4 380 873
	Microtube		5 242 956	2 930 415
	BloodCollectionTube		10 853 654	4 427 872